THE ASTROPHYSICAL JOURNAL, 439:875–904, 1995 February 1

NON-LTE LINE-BLANKETED MODEL ATMOSPHERES OF HOT STARS. I. HYBRID COMPLETE LINEARIZATION/ACCELERATED LAMBDA ITERATION METHOD

I. HUBENY[1] AND T. LANZ[2]
Laboratory for Astronomy and Solar Physics, NASA/Goddard Space Flight Center, Greenbelt, MD 20771
Received 1994 March 7; accepted 1994 August 4

ABSTRACT

A new numerical method for computing sophisticated non-LTE model stellar atmospheres is presented. The method, called the hybrid complete linearization/accelerated lambda iteration (CL/ALI) method, combines advantages of both its constituents. Its rate of convergence is virtually as high as for the standard CL method, while the computer time per iteration is almost as low as for the standard ALI method. The method is formulated as the standard complete linearization, the only difference being that the radiation intensity at selected frequency points is not explicitly linearized; instead, it is treated by means of the ALI approach. The scheme offers a wide spectrum of options, ranging from the full CL to the full ALI method. We demonstrate that the method works optimally if the majority of frequency points are treated in the ALI mode, while the radiation intensity at a few (typically two to 30) frequency points is explicitly linearized. We show how this method can be applied to calculate metal line–blanketed non-LTE model atmospheres, by using the idea of "superlevels" and "superlines" introduced originally by Anderson (1989). We calculate several illustrative models taking into account several tens of thousand of lines of Fe III to Fe VI and show that the hybrid CL/ALI method provides a robust method for calculating non-LTE line-blanketed model atmospheres for a wide range of stellar parameters. The results for individiual stellar types will be presented in subsequent papers in this series.

Subject headings: methods: numerical — radiative transfer — stars: atmospheres — stars: early-type

1. INTRODUCTION

Non-LTE line blanketing may be called "the last problem of classical stellar atmospheres." By a classical atmosphere we mean here a plane-parallel, horizontally homogeneous atmosphere in radiative and hydrostatic equilibrium. LTE stands for local thermodynamic equilibrium, and the term non-LTE loosely refers to any description allowing for some kind of departures from LTE, although in practice one usually means that number densities (populations) of some selected energy levels of some selected atoms and/or ions are allowed to depart from their LTE value. Finally, the term line blanketing encompasses a whole class of approaches whose common aim is to study the influence of thousands to millions of spectral lines on the resulting atmospheric structure and predicted emergent spectrum.

The problem of constructing line-blanketed model atmospheres is much easier assuming LTE, because the total line opacity is then a function of only two variables, the temperature and the electron density, and is therefore determined locally. Nevertheless, the very fact that we have to deal with millions of lines makes the problem nontrivial. One has to adopt some kind of statistical method. Indeed, the LTE line-blanketing problem may be relatively easily solved by introducing the *opacity distribution functions* (ODF), which represents a resampled total opacity in a given frequency interval. The effort in this area has culminated in a widely used grid of LTE line-blanketed model atmosphere by Kurucz (1979). Recently, Kurucz (1992) has updated this grid by considering more than 10^8 spectral lines for a model construction. There are also other methods of computing LTE line-blanketed models, which are generally based on some kind of Monte Carlo sampling of opacity in random frequencies (Peytremann 1974; Sneden, Johnson, & Krupp 1976). For an excellent review, see Carbon (1984).

On the other hand, in non-LTE, the individual spectral lines are allowed to contribute not only to total opacity, but also, via their radiative rates, to the global statistical equilibrium (i.e., determination of atomic level populations). Moreover, the lines of one species influence the radiative rates (mainly in bound-free transitions), and therefore the level populations, of other species. And, finally, since the level populations no longer depend only on local conditions, but also, again through the radiative transitions, on conditions in deeper layers, the problem is inherently nonlocal and highly nonlinear.

Do we really need to spend so much effort and computer resources to try to solve such an extremely difficult problem? One obvious answer is that if for nothing else, the non-LTE line-blanketed models may serve to justify the applicability of LTE models. But, more importantly, the experience gained from more than two decades of computing non-LTE model stellar atmospheres (for a summary of the first decade, see Mihalas 1978; the second decade is summarized, e.g., by Kudritzki & Hummer 1990; or in various papers in the volume edited by Crivellari, Hubeny, & Hummer 1991) has amply demonstrated that non-LTE effects play an important, even crucial, role in atmospheres of virtually all types of hot stars (effective temperature around 10,000 K and hotter). Yet, neglecting line blanketing introduces an uncertainty in the results, which in some cases casts doubt about the usefulness of non-LTE models in general. For instance, in the field of A and late-B stars, both main-sequence and chemically peculiar types, the non-LTE unblanketed models were successful in explaining some features in the far-UV continuum and line profiles of some strong lines (for a review, see Hubeny 1986), yet most workers in the field still keep using the Kurucz (1979) grid. The reason is that it is not

[1] Universities Space Research Association (USRA). E-mail: hubeny@stars.gsfc.nasa.gov.
[2] Fellow of the Swiss National Science Foundation. E-mail: lanz@stars.gsfc.nasa.gov.

a priori clear which is actually the greater evil—to neglect line blanketing or to neglect non-LTE effects. In many cases it appears that it is line blanketing which is the more important feature to be considered in models. One may somehow estimate the effect of neglecting it, but the only reliable solution to this dilemma is to produce non-LTE fully line-blanketed model atmospheres.

In the 1970s we have witnessed a period of rapid development of the field. The catalyst to the progress at this time was the method of complete linearization (CL), introduced by Auer & Mihalas (1969). The underlying concept of model construction became the realization that it is the (nonlocal) *coupling* of physical quantities (level populations, radiation field, temperature) which is the basic physical ingredient necessary to understand a stellar atmosphere. The complete linearization technique became the tool which, for the first time, actually allowed an explicit and fully consistent treatment of such a coupling. However, a high price had to be paid: due to limitations of the computer resources, only a very limited number of atomic levels and opacity sources (lines) could be treated. Since the computer time to run a model increases as a cube of the total number of unknowns, it soon became clear that regardless of how rapidly computer technology may have progressed, dealing with millions of lines within this framework was completely out of the question.

The 1980s witnessed a change in philosophy, namely a realization that not all varieties of coupling are equally important. In general, it became clear that only the essential part of the coupling has to be treated explicitly; the rest could be treated iteratively. In this respect, two concepts have been crucial for the further development. First, it was Anderson's (1985, 1987) realization that it is sufficient to group all frequency points into a small set of frequency blocks, rather than treating them separately. The method is called the multifrequency/multigray algorithm. After rearranging the frequencies into the blocks, the structural equations are still solved by complete linearization.

The second crucial point was the development of a whole class of approaches, generically referred to as accelerated lambda iteration (ALI) methods. Although based conceptually on work by Cannon (1973a, b) and Rybicki (1972), the realization of the full potential of ALI methods came only after the reformulation of these ideas by Scharmer (1982; for a complete review of this topic, including historical considerations, see, e.g., Rybicki 1991, or Hubeny 1992). Its basis is to express the radiation intensity through an approximate lambda operator acting on the source function plus a correction term known from the previous iteration. The radiation intensity is thus effectively eliminated from the set of unknown variables (see also § 2). The ALI formalism was first applied for constructing model stellar atmospheres by Werner (1986, 1987, 1989).

Although both above-mentioned methods represented a significant improvement over the previous approaches, they still could not be used directly to compute fully blanketed models because the number of lines treated was still rather limited (of the order of hundreds to thousands; and mostly lines of light elements like C, N, O). The limiting factor behind these approaches was that all the energy levels were treated separately. This prevented them from treating atoms with a very complex energy level structure, such as iron-peak elements. To solve this problem, Anderson (1989) introduced a statistical method, based on grouping many energy levels into a small numbr of "superlevels," and calculated the first truly blanketed non-LTE model atmospheres. Recently, Dreizler & Werner (1992, 1993) incorporated Anderson's idea into their ALI code and calculated several non-LTE line-blanketed model atmospheres for very hot stars.

In this series of papers, we will develop another method for computing non-LTE line-blanketed model atmospheres and present models for a wide range of stellar parameters. Is there a need for yet another method? In our opinion, the answer is definitely positive, for several reasons. First, our method combines advantages of its two basic ingredients, CL and ALI, namely a fast convergence rate (as in CL), and a short time per iteration (as in ALI). The most significant advantage of our method is that it allows us to choose from a wide spectrum of options, ranging from the essentially classical CL as formulated by Auer & Mihalas, to a full ALI code, as described by Werner (1987). We have found that somewhere between those two extremes the method works at its optimum, truly combining the advantages of CL (globalness and fast convergence rate), with ALI (speed of computation). Our computer program TLUSTY (Hubeny 1988; Hubeny & Lanz 1992) was modified to incorporate the present hybrid CL/ALI scheme. However, from the user's point of view, the corresponding changes are almost transparent.

Since line-blanketing non-LTE computer codes are enormously complicated (for instance, our program now contains more than 24,000 lines of code), it is virtually impossible to make sure that they are error free. Herein lies the second reason that an independently developed approach is worthwhile. The only way to verify the results, and therefore to give more credence to computed models, is to calculate models for the same stellar parameters, with the same species, levels, and transitions taken into account, by two completely independent methods and computer codes. In fact, we have begun the project of explicit and detailed comparison between the Kiel code (Dreizler & Werner 1993) and our code TLUSTY. The results of this study will be reported elsewhere.

The method will be described in detail in § 2. In § 3 we describe our statistical treatment of complicated energy level structure of iron-like species, and compare our approach to that of Anderson (1989) and Dreizler & Werner (1993). Some illustrative results are presented in § 4, and a discussion of the accuracy and reliability of the method is presented in § 5. The present paper, the first one in the series, concentrates mainly on a presentation and discussion of the method. The subsequent papers will be devoted to actual model results for individual stellar types. The first two classes to be studied in detail are hot, metal-rich DA white dwarfs (Lanz & Hubeny 1995, hereafter Paper II), and hot O subdwarfs.

2. THE HYBRID CL/ALI METHOD

2.1. *Formulation*

We begin with a brief summary of the classical complete linearization method. The classical stellar atmosphere problem, as specified in § 1, consists of solving the radiative transfer equation for a selected set of frequency points, the hydrostatic equilibrium equation, the radiative equilibrium equation, and the set of statistical equilibrium equations for chosen atomic energy levels. The set is closed by the equations of charge and particle conservation, together with definition equations for opacities, etc. (see Mihalas 1978

or Hubeny 1988). The equations are discretized in frequency and depth, which yields a set of highly coupled, nonlinear algebraic equations.

The physical state of an atmosphere may then be fully described by a set of vectors ψ_d for every depth point d, $d = 1, \ldots, \mathrm{ND}$, ND being the total number of depth points. The vector ψ_d is given by

$$\psi_d = \{J_1, \ldots, J_{\mathrm{NF}}, N, T, n_e, n_1, \ldots, n_{\mathrm{NL}}\} , \tag{1}$$

where J_i is the mean intensity of radiation in the ith frequency point, N is the total particle number density, T is the temperature, n_e is the electron density, and n_j is the number density (population) of level j; we have omitted the depth subscript d. The dimension of vector ψ_d is NN, NN = NF + NL + 3, NF is the number of frequency points, and NL is number of atomic energy levels. Strictly speaking, vector ψ_d should contain specific intensities of radiation, $I(\nu_i, \mu_k)$ (μ_k being discretized values of the directional cosines), instead of mean intensities $J(\nu_i)$. However, thanks to the variable Eddington factor technique (Auer & Mihalas 1970), a simplified form (eq. [1]) may be used.

The set of structural equations may be written formally as

$$\boldsymbol{P}(\boldsymbol{x}) = 0 , \tag{2}$$

where $\boldsymbol{x}$ is a vector formed from all vectors ψ_d, $\boldsymbol{x} = \{\psi_1, \ldots, \psi_{\mathrm{ND}}\}$; its dimension is therefore NN × ND.

The original complete linearization is nothing more than the Newton-Raphson method of solving equation (2), namely

$$\boldsymbol{x}^{(n+1)} = \boldsymbol{x}^{(n)} - J[\boldsymbol{x}^{(n)}]^{-1}\boldsymbol{P}[\boldsymbol{x}^{(n)}] , \tag{3}$$

where J is the Jacobi matrix (Jacobian), $J_{ij} = \partial P_i/\partial x_j$, i.e., the ij-element of the Jacobian is the derivative of the ith equation with respect to the jth unknown. Since the system (2) represents a *finite difference* solution of at most second-order differential equations (i.e., the Feautrier form of the transfer equation—see, for example, Mihalas 1978), the Jacobian J has a particularly simple structure, namely a block-tridiagonal form, and equation (2) is traditionally written (Mihalas 1978) as

$$-A_d^{(n)}\delta\psi_{d-1}^{(n)} + B_d^{(n)}\delta\psi_d^{(n)} - C_d^{(n)}\delta\psi_{d+1}^{(n)} = \boldsymbol{L}_d^{(n)} , \tag{4}$$

which now also indicates the explicit dependence of the matrices on the iteration number n. Here A, B, C are NN × NN matrices, and $\boldsymbol{L}_d^{(n)} = \boldsymbol{P}_d[\boldsymbol{x}^{(n)}]$ is the residuum vector (of dimension NN) at depth d.

Since the Jacobian is of a block-tridiagonal form, its inversion in equation (3) is not performed explicitly. Instead equation (3) is solved by applying a block-Gaussian elimination procedure, so we are left with inverting only one NN × NN matrix per depth point. Therefore, the total computer time for the ordinary complete linearization scales roughly as

$$N_{\mathrm{iter}} \times \mathrm{ND} \times \mathrm{NN}^3 . \tag{5}$$

As discussed in detail by Hubeny & Lanz (1992), one may reduce the total time either by reducing the time per iteration, or by reducing the number of iterations needed to achieve a certain accuracy, or both. They have suggested two methods for such a reduction. The first is the so-called Kantorovich method, which consists of keeping the Jacobian fixed after a few iterations, so that the costly matrix inversions are calculated only a few times. The second is an application of the so-called Ng acceleration, which reduces the number of iterations by using information not only from the previous iteration step, but also from several previous iterations. For a general review of these acceleration methods, see, e.g., Auer (1991).

In this paper, we will consider still another way of reducing the time per iteration, namely by reducing the size of the matrices to be inverted. There are several ways to achieve this:

1. The simplest approach is to linearize only those quantities which are "essential," while keeping the others fixed during linearization and updating them during a subsequent formal solution. Such an idea was implemented in the original version of the program TLUSTY. Specifically, this approach consists of keeping selected radiative transition rates "fixed." These fixed rates are calculated exactly in the formal solution step and are then held fixed during linearization. Subsequently, these rates are updated in the next formal solution step (this treatment differs from what is usually meant as "fixed" transitions by other authors, e.g., Auer, Heasley, & Milkey 1972, or Carlsson 1986, where the fixed rates are inherently approximate). By "formal solution" we mean a solution of *one equation at a time*, using current values of all other state parameters (for instance, solving the radiative transfer equation for given frequency for current values of the level populations, temperature, and electron density). The fixed rates approach has proved to be very useful for constructing model atmospheres with hundreds of atomic transitions taken into account, particularly if used in conjunction with the acceleration methods (Hubeny & Lanz 1992), but if too many transitions are taken in this mode, one basically recovers a lambda-iteration type of behavior, which is a serious drawback. In particular, the convergence rate is slow, and the solution tends to stablize rather than truly converge.

2. A much more sophisticated way of reducing the size of matrices to be inverted is the already mentioned Anderson multifrequency/multigray method. Basically, one substitutes

$$\{J_1, \ldots, J_{\mathrm{NF}}\} \rightarrow \{\bar{J}_1, \ldots, \bar{J}_{\mathrm{NB}}\} , \tag{6}$$

where $\bar{J}_i$ represents a mean intensity characteristic of ith frequency block, and NB is the number of blocks. In order to achieve a substantial reduction of time we have NB $\ll$ NF. Each block groups together all frequencies for which the radiation is formed in a similar way. It is not necessary that the block be composed of a continuous frequency interval (for instance, one block may represent all wings of weak lines, etc.; see Anderson 1985). The essence of the method consists of selecting appropriate frequency bands and the individual frequency points belonging to them. However, this is also a drawback of the method, since the bands have to be set essentially by hand.

3. In principle, the ALI method reduces the number of unknowns even more, because it eliminates *all* frequency points completely. This is achieved by expressing the mean intensity of radiation as

$$J_\nu^{(i)} = \Lambda_\nu^* S_\nu^{(i)} + (\Lambda_\nu - \Lambda_\nu^*) S_\nu^{(i-1)}, \tag{7}$$

where Λ_ν and Λ_ν^* are the exact and the approximate lambda operator, J_ν is the mean intensity of radiation, and S_ν is the source function, all at frequency ν. Superscript i indicates the iteration number. The mean intensity of radiation is thus represented by two terms. The second one, the "correction" term, is known from the previous iteration, while the first one represents an action of an approximate (and, therefore, simple) operator, Λ^*, on the source function, which is expressed as a function of temperature, density, and atomic level populations. The radiative transfer equations are thus eliminated from the coupled system of structural equations.

Equation (7) is particularly useful if the approximate operator Λ^* can be calculated easily. The real breakthrough was the demonstration by Olson, Auer, & Buchler (1986) that a nearly optimum Λ^* is simply a diagonal (or a simple multiband, like tridiagonal) part of the exact Λ operator. Finally, Rybicki & Hummer (1991) showed that the diagonal part of the exact lambda operator may be easily calculated within the framework of the Feautrier method. In the case of a diagonal (local) Λ^*, the first term of equation (7) is particularly simple—it is just a multiplication of the local source function by a real number. However, the basic problem is that when equation (7) is substituted into the statistical equilibrium, hydrostatic equilibrium, and radiative equilibrium equations, one still obtains a nonlinear system (see eq. [8]).

There are several ways to deal with such a nonlinearity. If one solves only the coupled radiative transfer + statistical equilibrium equations (sometimes called a *restricted non-LTE problem*), one may in principle avoid linearization by using the idea of *preconditioning* of the statistical equilibrium (Werner & Husfeld 1985; Herrero 1987; Rybicki & Hummer 1991, 1992), but it is not clear whether this approach may be applied to the more complicated stellar atmosphere problem. Werner (1986, 1989) therefore used a linearization approach. His approach solves the problem by using two nested iteration loops. The inner loop is a linearization loop which solves the nonlinear set of equations for the number densities and the temperature, while the outer loop is the true ALI iteration loop.

Here, we adopt a different approach. We divide all frequency points, chosen to represent accurately all lines and continua to be included in the model, into two groups. The first one contains the "crucial" frequency points (typically, a few frequencies near the important continuum edges, and the centers of the strongest lines) to be treated explicitly, i.e., to be fully linearized. The rest of frequency points comprise the so-called ALI points and are treated by means of the ALI formalism. This idea represents a significant generalization and improvement of our previous "fixed" frequency approach (Hubeny 1988). First, we use the ALI approach for frequency points previously called "fixed", and therefore the radiation field in these points is not fixed but is allowed to change via linearization of equation (7). Second, any transition, line or continuum, may generally be represented by a combination of explicit and ALI frequency points. Our formalism thus allows a totally arbitrary choice of the frequency-point partitioning, ranging from the fully ALI scheme (such as the Kiel code), to the original CL, where all points are explicit. As we will demonstrate numerically in § 4, the optimum choice lies between these two extremes. By choosing at least a few frequency points to be explicit, the time per iteration will increase somewhat, but the number of iterations will decrease dramatically.

We stress that the inclusion of more ALI frequencies does not lead to a significant increase of computer time in the linearization step. Obviously, the time for the formal solution increases with the number of frequency points considered, but the basic point is that since only one transfer equation is solved at a time, the increase of computer time is *linear* in the number of frequency points and not cubic as in the original CL.

2.2. *Equations*

In this paper, we will consider a diagonal Λ^*. An extension to a tridiagonal Λ^*, which is in principle straightforward, is underway, and will be reported in a future paper. We rewrite equation (7) as (dropping the superscript indicating the iteration number)

$$J_{j,d} = \Lambda_{j,d}^* \frac{\eta_{j,d}}{\kappa_{j,d}} + \Delta J_{j,d}^{\rm old}, \tag{8}$$

where j denotes the frequency index and d denotes the depth index. $\Lambda_{j,d}^*$ is simply a number. For numerical evaluation of $\Lambda_{j,d}^*$, we use here the procedure described by Rybicki & Hummer (1991), as well as the formulae of Olson & Kunasz (1987). We have found that both choices generally yield the same convergence rate, although in some cases the Rybicki & Hummer operator is preferred.

The source function $S_{j,d}$ is now written explicitly as the ratio of the emission coefficient $\eta_{j,d}$ over the absorption coefficient $\kappa_{j,d}$. In the following, we shall use a notation κ for the *thermal* absorption coefficient, and χ for the *total* absorption coefficient, $\chi_{j,d} = \kappa_{j,d} + n_{e,d}\sigma_e$, with $n_{e,d}\sigma_e$ being the electron scattering opacity; σ_e is the Thomson scattering cross section. In other words, the approximate Λ^* operator is defined through the thermal source function, not the total one. The second term on the right-hand side of equation (8) expresses $(\Lambda - \Lambda^*)S$ as $\Delta J^{\rm old}$, which is considered a known quantity and therefore is not linearized.

Equation (8) is linearized as follows:

$$\delta J_{j,d} = \Lambda_{j,d}^* \delta S_{j,d} = D_{j,d}^T \delta T_d + D_{j,d}^{n_e} \delta n_{e,d} + \sum_i D_{j,d}^i \delta n_{i,d}, \tag{9}$$

where

$$D_{j,d}^x = \Lambda_{j,d}^* \frac{\eta_{j,d}}{\kappa_{j,d}} \left(\frac{1}{\eta_{j,d}} \frac{\partial \eta_{j,d}}{\partial x} - \frac{1}{\kappa_{j,d}} \frac{\partial \kappa_{j,d}}{\partial x} \right), \tag{10}$$

represents the derivative of the mean intensity in the "ALI" frequency points with respect to temperature (for $x = T$), or electron density ($x = n_e$), or populations ($x = n_i$), i.e., $D^x_{j,d} = \partial J_{j,d}/\partial x_d$.

We stress that while $\Lambda^*_{j,d}$ is *fixed* during the linearization, it is updated after each completed iteration step. If we use the Olson & Kunasz formula, which expresses $\Lambda^*_{j,d}$ as an explicit function of monochromatic optical depth difference between the current depth point and its two immediate neighbors, we may, in principle, linearize even $\Lambda^*_{j,d}$. The work on implementing a linearization of Λ^* is underway and will be reported in a future paper.

2.2.1. *Radiative Equilibrium*

We write the radiative equilibrium equation in the form

$$\alpha\left[\int_0^\infty (\kappa_\nu J_\nu - \eta_\nu)d\nu\right] + \beta\left[\int_0^\infty \frac{d(f_\nu J_\nu)}{d\tau_\nu}\,d\nu - \frac{\sigma}{4\pi}T_{\rm eff}^4\right] = 0\,. \tag{11}$$

Here ν denotes frequency, f_ν is the Eddington factor, τ_ν is the monochromatic optical depth, σ is the Stefan-Boltzmann constant and $T_{\rm eff}$ is the effective temperature. α and β are empirical parameters. The two terms of equation (11) are in fact two equivalent forms of the radiative equilibrium equation (see, e.g., Mihalas 1978). The first one is the so-called integral form, expressing the fact that the total radiation energy emitted in the whole frequency range is equal to the total radiation energy absorbed. The second term, called the differential form, is the equivalent form expressing the constancy of total radiation flux with depth; the flux is expressed here through the variable Eddington factor $f_\nu = K_\nu/J_\nu$; K_ν being the second-order moment of the specific intensity. As discussed by Hubeny (1988), the differential form is more accurate at large depths, while the integral form is preferable at small depths. The previous versions of TLUSTY used for the radiative equilibrium the form (11), however with α and β given as a simple step function, namely $\alpha_d = 1$ and $\beta_d = 0$ for $d <$ NDRE, while $\alpha_d = 0$ and $\beta_d = 1$ for $d \geq$ NDRE, NDRE being an empirically chosen division point. In other words, the radiative equilibrium was considered at any depth point *either* as the integral form *or* as the differential form. We have found that a *linear combination* of both forms yields much better numerical stability and much higher accuracy of the total flux. Coefficients α and β are still arbitrary, and their optimum choice is a matter of some experimentation. We have found, however, that for virtually all stellar atmospheres the following choice provides good results, namely $\alpha = 1$ everywhere but a few (one to five) innermost depth points, while

$$\beta = \begin{cases} 0\,, & \text{for } \tau_{\rm Ross} < \tau_{\rm div}\,; \\ 1\,, & \text{elsewhere} \end{cases}, \tag{12}$$

with $\tau_{\rm div} \approx 1$, $\tau_{\rm Ross}$ being the Rosseland mean opacity. This means that for $\tau > \tau_{\rm div}$, both forms are allowed to contribute equally, which increases the accuracy and stability considerably. We have also experimented with other choices of α and β (as for instance choosing α and β to yield both terms with a similar numerical value, or being specified as various functions of $\tau_{\rm Ross}$), but these were not found to be significantly better than equation (12).

Equations (11) and (12) improve the accuracy of computed models regardless of whether one employs the traditional CL or any other method. In case of the hybrid CL/ALI method, the linearization of equation (11) is as follows. We first rewrite equation (11) in a discretized form, viz.,

$$\alpha_d\left[\sum_i^{\rm NFEXP} w_{i,d}(\kappa_{i,d}J_{i,d} - \eta_{i,d}) + \sum_j^{\rm NFALI} w_{j,d}(\kappa_{j,d}J_{j,d} - \eta_{j,d})\right] + \beta_d\left(\sum_i^{\rm NFEXP} w_{i,d}\frac{f_{i,d}J_{i,d} - f_{i,d-1}J_{i,d-1}}{\Delta\tau_{i,d-1/2}} + \sum_j^{\rm NFALI} w_{j,d}\frac{f_{j,d}J_{j,d} - f_{j,d-1}J_{j,d-1}}{\Delta\tau_{j,d-1/2}} - \frac{\sigma}{4\pi}T_{\rm eff}^4\right) = 0\,, \tag{13}$$

where

$$\Delta\tau_{i,d-1/2} = \frac{1}{2}(m_d - m_{d-1})\left(\frac{\chi_{i,d}}{\rho_d} + \frac{\chi_{i,d-1}}{\rho_{d-1}}\right), \tag{14}$$

ρ being the density. In other words, each integral over frequency is replaced by two quadrature sums: one over the "explicit" frequency points, and the second one over the "ALI" points. We denote the former points with the subscript i and the latter with j. The total number of these points is NFEXP and NFALI, respectively. Notice that the frequency quadrature weights w_i and w_j are allowed to be depth dependent. This reflects the fact that allowing for a general depth-dependent absorption profile for lines necessitates introducing depth-dependent quadrature weights, due to the requirement of preserving the exact numerical normalization of the absorption profile at every depth.

The essential feature is that the radiation intensity in the ALI points is expressed by equation (8). We will not write this expanded form of equation (13); we merely point out that the summation over the ALI points in the integral form part of equation (13) (the second summation on the left-hand side) is written as

$$\sum_j^{\rm NFALI} w_{j,d}[\kappa_{j,d}\Delta J^{\rm old}_{j,d} + (\Lambda^*_{j,d} - 1)\eta_{j,d}]\,, \tag{15}$$

which in fact represents a *preconditioning* of the radiative equilibrium equation.

Linearization of equation (13) is straightforward, though rather cumbersome. Let us denote the left-hand side of equation (13) as R_d. The linearized form then reads

$$\sum_{i}^{\mathrm{NFEXP}} \frac{\partial R_d}{\partial J_{i,d}} \delta J_{i,d} + \frac{\partial R_d}{\partial T_d} \delta T_d + \frac{\partial R_d}{\partial N_d} \delta N_d + \frac{\partial R_d}{\partial n_{e,d}} \delta n_{e,d} + \sum_{l}^{NL} \frac{\partial R_d}{\partial n_{l,d}} \delta n_{l,d} + \sum_{i}^{\mathrm{NFEXP}} \frac{\partial R_d}{\partial J_{j,d-1}} \delta J_{j,d-1}$$
$$+ \frac{\partial R_d}{\partial T_{d-1}} \partial T_{d-1} + \frac{\partial R_d}{\partial N_{d-1}} \partial N_{d-1} + \frac{\partial R_d}{\partial n_{e,d-1}} \delta n_{e,d-1} + \sum_{l}^{NL} \frac{\partial R_d}{\partial n_{l,d-1}} \delta n_{l,d-1} = -R_d \,, \tag{16}$$

where

$$\frac{\partial R_d}{\partial J_{i,d}} = \alpha_d w_{i,d} \kappa_{i,d} + \beta_d w_{i,d} \frac{f_{i,d}}{\Delta\tau_{i,d-1/2}} \,, \tag{17}$$

and, for example,

$$\frac{\partial R_d}{\partial T_d} = \alpha_d \left\{ \sum_{i}^{\mathrm{NFEXP}} w_{i,d} \left(\frac{\partial \kappa_{i,d}}{\partial T_d} J_{i,d} - \frac{\partial \eta_{i,d}}{\partial T_d} \right) + \sum_{j}^{\mathrm{NFALI}} w_{j,d} \left[\frac{\partial \kappa_{j,d}}{\partial T_d} \Delta J_{j,d}^{\mathrm{old}} + \frac{\partial \eta_{j,d}}{\partial T_d} (\Lambda_{j,d}^{*} - 1) \right] \right\} + \beta_d [\gamma_T^{\mathrm{EXP}} + \gamma_T^{\mathrm{ALI}}] \,, \tag{18}$$

where

$$\gamma_T^{\mathrm{EXP}} = -\frac{1}{2} (m_d - m_{d-1}) \sum_{i}^{\mathrm{NFEXP}} w_{i,d} \frac{f_{i,d} J_{i,d} - f_{i,d-1} J_{i,d-1}}{(\Delta\tau_{i,d-1/2})^2} \frac{\chi_{i,d}}{\rho_d} \frac{\partial \chi_{i,d}}{\partial T_d} \,, \tag{19}$$

$$\gamma_T^{\mathrm{ALI}} = \frac{1}{2} (m_d - m_{d-1}) \sum_{j}^{\mathrm{NFALI}} \frac{w_{j,d}}{\Delta\tau_{j,d-1/2}} \left[f_{j,d} D_{j,d}^{T} - (f_{j,d} J_{j,d} - f_{j,d-1} J_{j,d-1}) \frac{1}{\rho_d \Delta\tau_{j,d-1/2}} \frac{\partial \chi_{j,d}}{\partial T_d} \right] . \tag{20}$$

Analogous expressions can be derived for other partial derivatives in equation (16), replacing the derivatives of the absorption and emission coefficient with respect to temperature by the appropriate derivatives.

2.2.2. *Hydrostatic Equilibrium Equation*

The hydrostatic equilibrium equation reads

$$\frac{dP}{dm} = g \,, \tag{21}$$

where g is the surface gravity and P is the total pressure. The latter is given by

$$P = P_{\mathrm{gas}} + P_{\mathrm{turb}} + P_{\mathrm{rad}} \,, \tag{22}$$

i.e., as a sum of the gas, turbulent, and radiation pressure, respectively. All terms except the radiation pressure are linearized quite analogously to the original CL (see Mihalas 1978; or Mihalas, Heasley, & Auer 1975, hereafter MHA). The radiation pressure is written again as a sum of the "explicit" and the "ALI" contributions, viz.,

$$\frac{c}{4\pi} P_{\mathrm{rad}} = \sum_{i}^{\mathrm{NFEXP}} w_{i,d} f_{i,d} J_{i,d} + \sum_{j}^{\mathrm{NFALI}} w_{j,d} f_{j,d} \left(\Lambda_{j,d}^{*} \frac{\eta_{j,d}}{\kappa_{j,d}} + \Delta J_{j,d}^{\mathrm{old}} \right) . \tag{23}$$

Linearization of these equations is straightforward.

2.2.3. *Statistical Equilibrium Equations*

The same idea is also applied to the equations of statistical equilibrium. The equations are written formally as (Mihalas 1978, p. 137–145)

$$\boldsymbol{A}\boldsymbol{n} = \boldsymbol{b} \,, \tag{24}$$

where A is the rate matrix, $\boldsymbol{n}$ is the vector of populations, and $\boldsymbol{b}$ is the right-hand side vector. We are not interested here in the rows of the rate matrix corresponding to the respective last equations for each individual species (the abundance definition equation, or the charge or particle conservation equation). These rows do not depend explicitly on radiation, and therefore they are linearized in exactly the same way as in the standard CL. The elements of the rate matrix corresponding to the true statistical equilibrium equation are given by

$$A_{ij} = -(R_{ji} + C_{ji}) \,, \qquad \text{for} \quad i \neq j; \qquad A_{ii} = \sum_{m=i} (R_{im} + C_{im}) \,, \tag{25}$$

where R_{ij} and C_{ij} are the radiative and collisional rates for the transition $i \rightarrow j$, respectively. The radiative rates are given by (assuming $i < j$)

$$R_{ij} = \int \frac{4\pi}{h\nu} \sigma_{ij}(\nu) J_\nu \, d\nu \,, \tag{26}$$

and

$$R_{ji} = \int \frac{4\pi}{h\nu} \sigma_{ij}(\nu) G_{ij}(\nu) \left(\frac{2h\nu^3}{c^2} + J_\nu \right) d\nu \,, \tag{27}$$

where σ is the absorption cross section, and

$$G_{ij}(\nu) = \begin{cases} g_i/g_j \,, & \text{for a line transition ;} \\ n_e \Phi_i \exp(-h\nu/kT) \,, & \text{for a continuum transition ,} \end{cases} \tag{28}$$

where g is the statistical weight and Φ the Saha-Boltzmann factor.

After the original suggestion by Auer & Mihalas (1969), one does not linearize equation (24) directly; instead one linearizes

$$\boldsymbol{n} - A^{-1}\boldsymbol{b} = 0 \,. \tag{29}$$

which yields

$$\frac{\partial \boldsymbol{n}}{\partial x} = - A^{-1} V_x \,, \tag{30}$$

This quantity represents the column of the Jacobi matrix corresponding to quantity x; x stands for any quantity of vector ψ defined by equation (1). Here

$$V_x = \frac{\partial A}{\partial x} \boldsymbol{n} - \frac{\partial \boldsymbol{b}}{\partial x} \,. \tag{31}$$

In the case of the standard CL, the corresponding expressions were given by MHA. Let the transition $l \rightarrow u$ be represented by an arbitrary combination of the "explicit" and "ALI" frequency points; either subset is allowed be empty. Generally, the contribution from this transition comes only to the two following components of vector V_x, namely

$$(V_x)_l = \frac{\partial (R_{lu} + C_{lu})}{\partial x} n_l - \frac{\partial (R_{ul} + C_{ul})}{\partial x} n_u \,. \tag{32}$$

and

$$(V_x)_u = - (V_x)_l \,. \tag{33}$$

The radiative rate is written in a discretized form as

$$R_{lu} = \frac{4\pi}{h} \left[\sum_i^{\text{NFEXP}} w_i \frac{\sigma_{lu}(\nu_i)}{\nu_i} J_i + \sum_j^{\text{NFALI}} w_j \frac{\sigma_{lu}(\nu_j)}{\nu_j} J_j \right], \tag{34}$$

and analogously for the downward rate. The contribution from the collisional rates and from the "explicit" frequency points is the same as in the standard Cl, while the ALI contribution is given by

$$(V_x)_l^{\text{ALI contrib}} = [n_l - n_u G_{lu}(\nu_j)] \frac{4\pi}{h} \sum_j^{\text{NFALI}} w_j \frac{\sigma_{lu}(\nu_j)}{\nu_j} D_j^x \,, \tag{35}$$

where D_j^x is given by equation (10). The important difference from the standard complete linearization is that because the derivatives D_j^x are generally nonzero for x being the individual level populations, the Jacobian contains contributions from the populations. This of course expresses the already stated fact that within the ALI formalism the statistical equilibrium equations are no longer linear in populations.

3. NON-LTE OPACITY DISTRIBUTION FUNCTIONS

3.1. *Concept of Superlevels*

The method described above improves considerably the treatment of transitions which are not fully linearized. Even very complicated problems may now be easily solved by linearizing the radiation intensities in only a few frequency points in the most important transitions, while treating the rest of frequency points by means of ALI. However, this approach is still not sufficient for treating atoms with a very complicated energy level structure, as for instance the iron peak elements. Indeed, one would have to deal with about 10^4–10^5 energy levels, and consequently with 10^6–10^7 transitions, which is clearly beyond the capacity of even the most powerful computers. Therefore, the only way of dealing with this situation is through some statistical approach. In the context of non-LTE models atmospheres, such an approach was developed by Anderson (1989), and later used by Dreizler & Werner (1992, 1993) and, with a slightly different flavor, by Hubeny, Hummer, & Lanz (1994).

The idea consists of grouping several (many) individual energy levels together, forming the so-called superlevel. The basic physical assumption is that all real levels j forming the superlevel J have a common non-LTE departure coefficient, or, in other words, all components j are in Boltzmann equilibrium with respect to each other. There is a certain flexibility in choosing a particular partitioning of individual levels into superlevels, but the choice is ultimately constrained by two opposing requirements: (1) the energies of the individual components should be close; the levels should have similar physical properties (e.g., belonging to the same

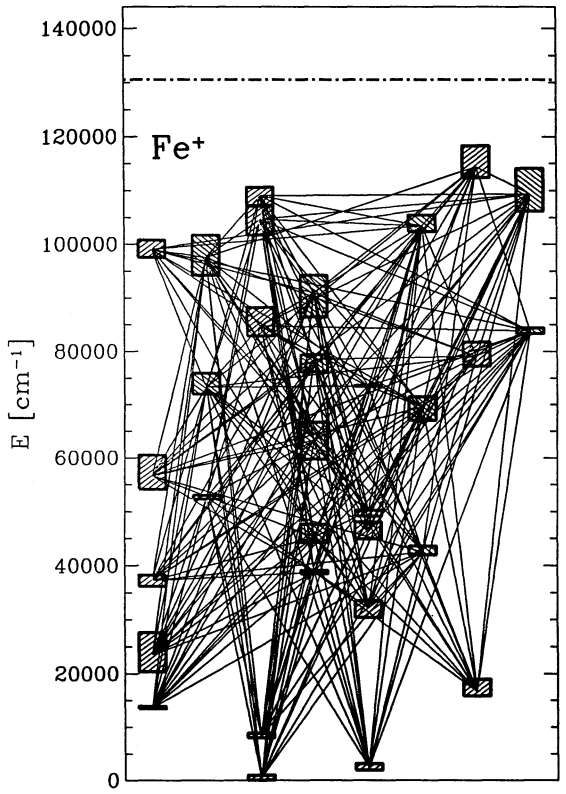

FIG. 1a

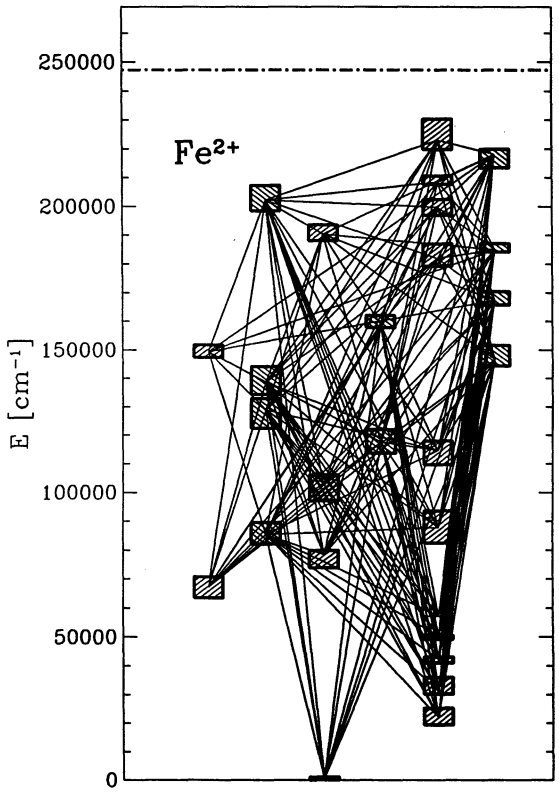

FIG. 1b

FIG. 1.—Superlevels (shown by boxes) and the corresponding superlines (shown by connecting lines) for our adopted models of various ions of iron: (*a*) Fe II; (*b*) Fe III; (*c*) Fe IV; (*d*) Fe V; (*e*) Fe VI. The ordinate represents the level energy in cm^{-1}; the height of a box indicates the real spread of energies of the inividual energy levels forming a given superlevel. The dot-dashed line near the top indicates the ionization energy of the given ion. The position on the *x*-axis does not have particular meaning, except that we have arranged the superlevels into columns with alternating parity; the first, third, etc., columns are even levels; the second, fourth, etc., columns are odd levels. Also, the boxes are thatched by lines with a positive slope for the even levels, and by a negative slope for the odd levels. We stress that only levels with *measured energies* (i.e., not predicted levels) are considered in the construction of superlevels

spectroscopic multiplet; having the same parity, etc.); and (2) there should not be too many superlevels, which would defeat the purpose of the statistical approach.

Anderson (1989) and Dreizler & Werner (1993) have partitioned the true levels into the individual superlevels on the basis of the level energies only, resulting in a rather small number, typically seven to eight, of superlevels per ionization degree. Although this approach has the obvious advantage of keeping the total number of energy levels, and therefore equations to be solved, as small as possible, there are several drawbacks:

(1) Since the energy widths of the superlevels are rather wide, the corresponding transitions between them span wide frequency intervals. If the radiation is formed in disparate parts of the spectrum, its behavior may be quite different, which may violate the equality of the *b*-factors for individual components.

(2) Since the approach does not distinguish between radiatively decaying and metastable states, the assumption of equal *b*-factors of all components may again be questionable, for the lowest superlevels in particular.

(3) One has to consider radiative transitions between individual components of the same superlevel. Although not serious, this feature may be inconvenient from the point of view of coding since one has to allow for radiative transitions from each superlevel to itself.

Therefore, we have decided to base our partitioning scheme on the following criteria: (1) all levels within a superlevel have the same parity; (2) energy differences between levels are small. The actual choice is made by inspecting the distribution of the individual excitation energies for levels in the even and the odd parity system, looking for clustering of energies. We select typically 10–15 superlevels per system, which means about 20–30 superlevels per ion. For illustration, we present in Figures 1*a*–1*e* the superlines and corresponding superlevels of several ions of iron, Fe II to Fe VI, which we feel represent reasonable starting models for these ions. The detailed properties of the superlevels (parity, statistical weight, mean energy, and energy ranges are given in Tables 1–5 for Fe II to Fe VI. These are the model atoms used in model atmosphere calculations reported here (§ 4). We plan to undertake a detailed study of the sensitivity of resulting model atmospheres to various choices of superlevel partitioning; the results will be reported in a future paper.

We stress that only levels with *measured energies* (i.e., not predicted levels) are considered in the construction of superlevels. An inspection of Figures 1*a*–1*e* indicates that we will miss many high-energy levels. We treat these levels through the "upper sums" calculated by means of the appropriate partition function, as described by Hubeny (1988, § 4.7). For the iron partition functions, we

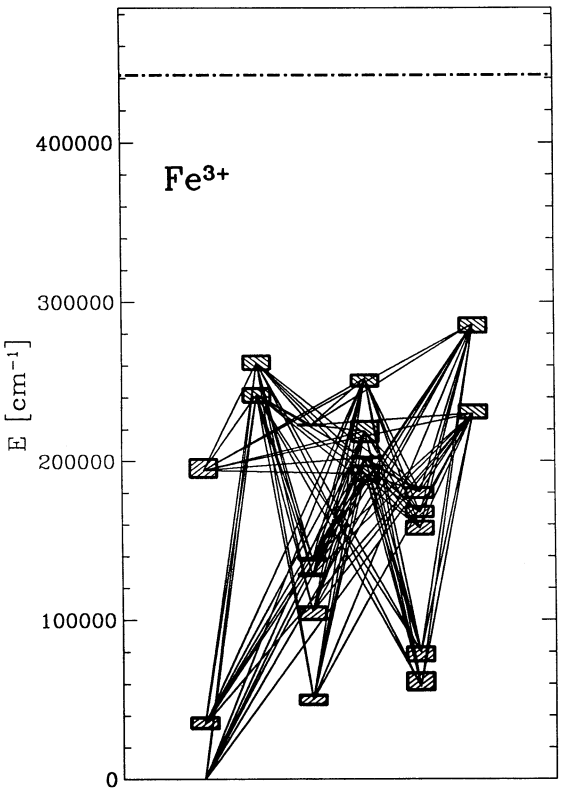

FIG. 1c

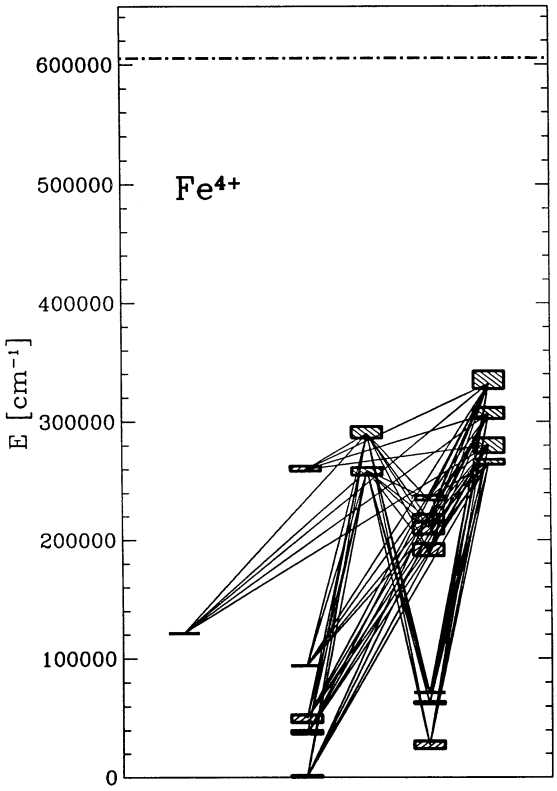

FIG. 1d

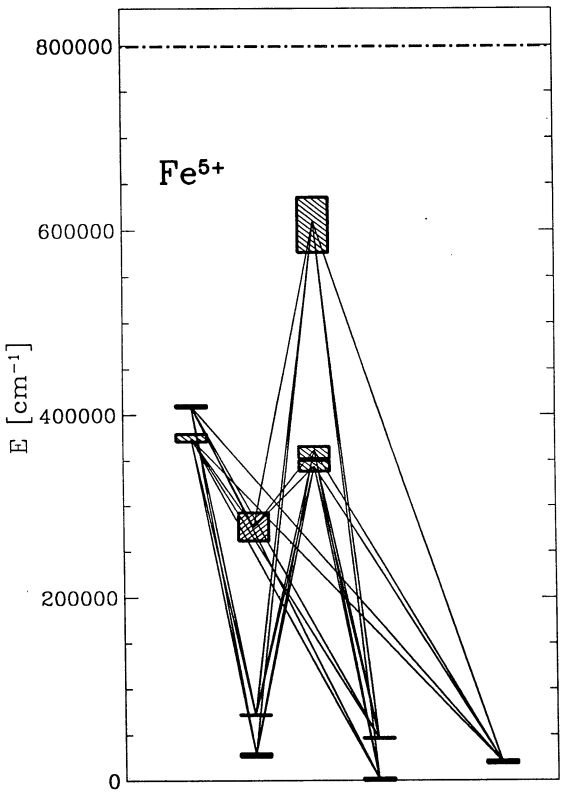

FIG. 1e

TABLE 1

MODEL ATOM FOR Fe II

I	Parity	g_I	E_I (cm^{-1})	E_{min} (cm^{-1})	E_{max} (cm^{-1})
1	Even	30.	416.3	0.	977.
2	Even	28.	2416.6	1873.	3117.
3	Even	20.	8320.5	7955.	8847.
4	Even	12.	13612.4	13474.	13905.
5	Even	24.	16692.4	15845.	18887.
6	Even	200.	23432.3	20340.	27620.
7	Even	96.	32115.7	30389.	33501.
8	Even	22.	37196.4	36126.	38215.
9	Odd	30.	38709.8	38459.	39109.
10.....	Odd	60.	42438.9	41968.	43621.
11.....	Odd	60.	45224.7	44233.	47626.
12.....	Even	24.	46159.6	44915.	48039.
13.....	Even	40.	50043.6	49101.	50213.
14.....	Odd	24.	52671.4	52299.	52966.
15.....	Even	106.	56624.9	54063.	60445.
16.....	Odd	494.	63258.6	59663.	66672.
17.....	Odd	106.	69535.9	67001.	71433.
18.....	Odd	192.	73227.4	71965.	75915.
19.....	Even	28.	73457.1	73394.	73637.
20.....	Odd	54.	78469.0	76129.	79332.
21.....	Even	92.	79041.0	77231.	81735.
22.....	Odd	28.	83778.7	83305.	84360.
23.....	Even	250.	84714.7	82854.	88189.
24.....	Odd	584.	90920.4	86389.	94190.
25.....	Odd	246.	97542.1	94212.	101707.
26.....	Even	122.	99039.9	97507.	100750.
27.....	Odd	528.	103431.3	102340.	105408.
28.....	Even	950.	104626.3	101698.	107066.
29.....	Even	382.	108973.7	107176.	110612.
30.....	Odd	916.	109335.9	106120.	114104.
31.....	Even	220.	114353.5	112397.	118277.

TABLE 2

MODEL ATOM FOR Fe III

I	Parity	g_I	E_I (cm^{-1})	E_{min} (cm^{-1})	E_{max} (cm^{-1})
1	Even	25.	422.9	0.	1027.
2	Even	90.	21928.5	19405.	25142.
3	Even	50.	31176.5	30089.	35804.
4	Even	12.	42106.5	41000.	42897.
5	Even	30.	50180.5	49148.	50412.
6	Even	9.	57221.7	57222.	57222.
7	Even	112.	67029.5	63425.	70729.
8	Even	63.	78311.2	73728.	79860.
9	Odd	36.	85297.4	82002.	89491.
10.....	Even	218.	87755.5	82383.	93513.
11.....	Even	25.	102560.0	97041.	105929.
12.....	Even	41.	114549.0	109571.	117950.
13.....	Odd	305.	117485.4	113584.	121950.
14.....	Odd	272.	128726.7	122347.	132785.
15.....	Odd	501.	138512.3	134265.	144117.
16.....	Odd	134.	146621.6	144332.	151637.
17.....	Even	72.	149284.3	147282.	151758.
18.....	Odd	53.	158988.5	157684.	162085.
19.....	Odd	144.	167214.4	165719.	170311.
20.....	Even	451.	181941.1	179179.	186999.
21.....	Odd	104.	185027.0	184181.	187090.
22.....	Even	139.	190304.3	188013.	193611.
23.....	Even	174.	199789.8	196881.	202429.
24.....	Odd	457.	202148.5	198334.	207273.
25.....	Even	147.	208441.0	207641.	210615.
26.....	Odd	284.	218098.9	213458.	219781.
27.....	Even	434.	222888.3	219740.	230257.

TABLE 3

MODEL ATOM FOR Fe IV

I	Parity	g_I	E_I (cm^{-1})	E_{min} (cm^{-1})	E_{max} (cm^{-1})
1	Even	6.	0.0	0.	0.
2	Even	68.	34752.8	32246.	38938.
3	Even	78.	50281.6	47079.	52838.
4	Even	56.	58283.9	56058.	66720.
5	Even	28.	79761.2	74097.	82897.
6	Even	16.	105200.6	100118.	108258.
7	Even	30.	128480.3	127766.	128968.
8	Even	20.	138399.2	137701.	138844.
9	Even	162.	157563.1	153652.	162088.
10.....	Even	94.	167475.2	164951.	171476.
11.....	Even	24.	180607.3	177006.	183164.
12.....	Odd	130.	192218.9	187879.	196847.
13.....	Even	78.	194380.1	189975.	201212.
14.....	Odd	20.	202379.8	201919.	202608.
15.....	Odd	522.	218981.5	212136.	224871.
16.....	Even	10.	222845.0	222841.	222852.
17.....	Odd	246.	229974.5	226852.	234984.
18.....	Odd	60.	241742.0	236919.	245742.
19.....	Odd	130.	252025.4	246991.	254169.
20.....	Odd	114.	261969.6	257503.	266335.
21.....	Odd	30.	286203.1	280758.	289819.

TABLE 4

MODEL ATOM FOR Fe V

I	Parity	g_I	E_I (cm^{-1})	E_{min} (cm^{-1})	E_{max} (cm^{-1})
1	Even	25.	787.2	0.	1283.
2	Even	90.	27158.9	24055.	30430.
3	Even	38.	37040.6	36586.	39633.
4	Even	12.	50048.7	46291.	52733.
5	Even	30.	62324.5	61854.	63420.
6	Even	9.	71280.3	71280.	71280.
7	Even	5.	93832.3	93832.	93832.
8	Even	1.	121130.2	121130.	121130.
9	Even	56.	190784.1	186434.	196839.
10.....	Even	68.	210058.2	204730.	214611.
11.....	Even	67.	217926.4	215783.	221305.
12.....	Even	28.	234781.7	233634.	237730.
13.....	Odd	120.	258674.5	254803.	261180.
14.....	Even	20.	259551.8	258434.	262509.
15.....	Odd	48.	265802.9	263899.	267929.
16.....	Odd	227.	280439.8	273643.	285962.
17.....	Odd	180.	289842.6	286155.	295973.
18.....	Odd	84.	306781.8	302293.	311539.
19.....	Odd	60.	332045.8	327534.	342462.

TABLE 5

MODEL ATOM FOR Fe VI

I	Parity	g_I	E_I (cm^{-1})	E_{min} (cm^{-1})	E_{max} (cm^{-1})
1	Even	28.	1163.6	0.	2001.
2	Even	30.	20299.7	18738.	21315.
3	Even	38.	28445.9	26215.	29203.
4	Even	14.	46382.9	46217.	46604.
5	Even	10.	71844.1	71708.	72049.
6	Even	88.	276583.1	261841.	292330.
7	Odd	126.	343351.5	338256.	350018.
8	Odd	86.	361623.5	351806.	365494.
9	Odd	52.	374135.0	370538.	379078.
10.....	Odd	6.	409662.1	408207.	410390.
11.....	Odd	102.	609822.2	575930.	635430.

use tables of Sparks & Fischel (1971). To verify the reliability of this approach, we have set up extended model atoms with two additional superlevels per ion, with one superlevel for each parity system, representing all the higher (predicted) levels. The data for predicted levels were taken from Kurucz (1991). We have performed several test calculations and verified that the populations of the two additional superlevels are consistent with the predictions based on the Sparks & Fischel partition functions.

3.2. *Concept of Superlines*

In the following we denote by lower-case letters i and j the genuine energy levels (eigenstates), while the superlevels are denoted by upper-case letters I and J. We adopt the convention that the superlevel I is formed of several levels i. The population of superlevel I is given by

$$n_I = \sum_i n_i \,, \tag{36}$$

where n_i are populations of the individual components in the superlevel I. Other quantities describing a superlevel may be defined in several ways. Our definitions differ slightly from those adopted by Anderson (1989) and Dreizler & Werner (1993). The reason is that we are going to apply the occupation probability formalism, as described in Hubeny et al. (1994). The statistical weight of level I is defined by

$$g_I = \sum_i g_i \,, \tag{37}$$

and therefore is a depth-independent quantity, in contrast to Anderson's (1989) definition. The depth dependence, which arises due to the fact that the energies of individual levels with a superlevel are not identical, is absorbed in our formalism within the superlevel occupation probability, defined as

$$w_I = \frac{\exp\,(E_I/kT)}{g_I} \sum_i g_i w_i \exp\left(-\frac{E_i}{kT}\right), \tag{38}$$

where the averaged energy is defined by

$$E_I = \frac{\sum_i g_i w_i E_i \exp\,(-E/kT)}{\sum_i g_i w_i \exp\,(-E_i/kT)} \,. \tag{39}$$

The quantity w_i is the occupation probability of level i, i.e., the probability that the atom in question is in state i relative to that in a similar ensemble of noninteracting atoms. Correspondingly, $(1 - w_i)$ is the probability that the state i is dissolved. The standard formalism is recovered by putting $w_i = 1$ for all states i. To avoid confusion we stress that in our formalism the superlevel occupation probability w_I is a formal quantity whose interpretation is not analogous to that of ordinary occupation probabilities. As follows from equation (38), w_I may be different from unity even if all $w_i = 1$; in fact in order to recover $w_I \to 1$ we need also $E_i \to E_I$ for all i, i.e., all the energy levels forming a superlevel having energies which are close enough.

The most important quantities are the absorption and emission cross sections for the transitions between the individual superlevels, i.e., the superlines. Generally, the true absorption coefficient in the transition $I \to J$ (i.e., not corrected for stimulated emission) is given by (see Hubeny et al. 1994)

$$\chi_{IJ}(\nu) = \sum_i \sum_j n_i w_j \sigma_{ij}(\nu) \,, \tag{40}$$

where $\sigma_{ij}(\nu)$ is the cross section for the (ordinary) transition $i \to j$. We note that the line absorption cross section is given by

$$\sigma_{ij}(\nu) = \frac{\pi e^2}{mc} f_{ij}\, \phi_{ij}(\nu) \,, \tag{41}$$

where f_{ij} is the oscillator strength, and $\phi_{ij}(\nu)$ is the (normalized) absorption profile, given by

$$\phi_{ij}(\nu) = \frac{1}{\sqrt{\pi}\,\Delta\nu_{\rm D}} H\left[\frac{\Gamma_{ij}}{(4\pi\,\Delta\nu_{\rm D})}\,,\ \frac{(\nu - \nu_{ij})}{\Delta\nu_{\rm D}}\right], \tag{42}$$

where $H(a, v)$ is the Voigt function, ν_{ij} is the line center frequency, $\Delta\nu_{\rm D}$ is the Doppler width, and Γ_{ij} the damping parameter for the transition $i \to j$. Other quantities have their usual meanings.

Within the superlevel formalism, the absorption coefficient for transition $I \to J$ has to be expressed as

$$\chi_{IJ}(\nu) = n_I w_J \sigma_{IJ}(\nu) \,. \tag{43}$$

Using equations (38), (40), and (43), we find that the absorption cross section has to be given by

$$\sigma_{IJ}(\nu) = \frac{g_J \exp\,(-E_J/kT) \sum_i \sum_j g_i w_i w_j \sigma_{ij}(\nu) \exp\,(-E_i/kT)}{[\sum_i g_i w_i \exp\,(-E_i/kT)][\sum_j g_j w_j \exp\,(-E_j/kT)]} \,. \tag{44}$$

Similarly, from the definition of the emission coefficient, viz.,

$$\frac{c^2}{2h\nu^3}\,\eta_{JI}(\nu) = \sum_i \sum_j n_j w_i \left(\frac{g_i}{g_j}\right)\sigma_{ij}(\nu) = n_J w_I \left(\frac{g_I}{g_J}\right)\sigma_{JI}(\nu) \,, \tag{45}$$

we obtain for the emission cross section

$$\sigma_{JI}(\nu) = \frac{g_J \exp(-E_I/kT) \sum_i \sum_j g_i w_i w_j \sigma_{ij} \exp(-E_j/kT)}{[\sum_i g_i w_i \exp(-E_i/kT)][\sum_j g_j w_j \exp(-E_j/kT)]} . \quad (46)$$

The absorption and emission cross-sections are generally different. They would be equal if $E_J + E_i = E_I + E_j$, i.e., $E_J - E_I = E_j - E_i$, i.e., if the frequencies of all transitions forming a superline are equal. Since we construct the superlevels to be composed of levels of nearly equal energy, the approximation $\sigma_{IJ}(\nu) \simeq \sigma_{JI}(\nu)$ is usually well justified.

To complete our formalism, we give expressions for the photoionization cross sections from the superlevels and for the collisional rates between superlevels. The photoionization cross section is given by

$$\sigma_{I\kappa}(\nu) = \frac{\sum_i g_i w_i \sigma_{i\kappa}(\nu) \exp(-E_i/kT)}{\sum_i g_i w_i \exp(-E_i/kT)} . \quad (47)$$

The collisional rates are given by expressions analogous to equations (44), (46) and (47), replacing σ by C everywhere.

3.3. *Numerical Treatment of the Superline Cross Sections*

The absorption cross section as defined by equation (44) is a very complicated and highly nonmonotonic function of frequency. To illustrate this, we plot in Figure 2 a typical cross section (transition 1 to 13 of Fe III). The upper panel shows the actual cross section, which was calculated using some 14,500 frequency points (the lower panel will be discussed later). Nevertheless, the actual

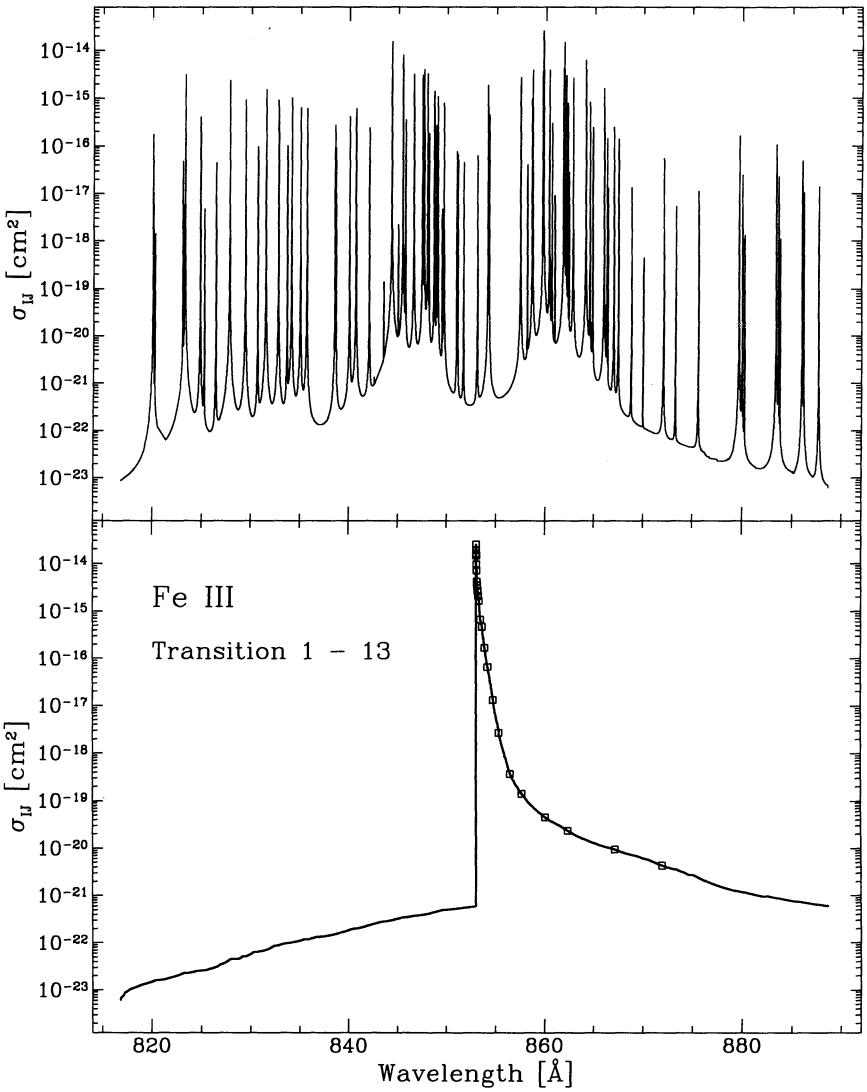

FIG. 2.—A typical superlevel cross section: transition 1 to 13 of Fe III. The upper panel shows the actual cross-section, calculated for T = 19,221 K, n_e = 1.06 × 10^{14} cm^{-3}. The total of 15,485 frequency points were used in the evaluation of the cross section. The lower panel shows the corresponding opacity distribution function, constructed as discussed in the text. Small squares (a total of 24) indicate the frequency points used to represent this ODF in model atmosphere calculations

form of the cross section does not matter. The only quantities which do matter are the corresponding *integrals* over the frequency range covered by a superline; the integrals may represent for instance the radiative equilibrium integrand, $\kappa(\nu)J_\nu - \eta(\nu)$, or the integrand occurring in evaluating radiative rates (schematically) $\sigma(\nu)J_\nu$. This observation forms the basis of the statistical approach.

In order to facilitate the subsequent discussion, we write the integrals to be dealt with as

$$\int_{\nu_0}^{\nu_1} f(\nu)J_\nu d\nu , \tag{48}$$

where ν_0 and ν_1 are the minimum and maximum frequency within a superline, and $f(\nu)$ is a function of frequency which depends on the particular integral under study; $f(\nu)$ always contains the superline cross section $\sigma(\nu)$. The treatment of expression (48) is difficult because there is another wildly varying function of frequency besides $f(\nu)$, and that is J_ν. More accurately, J_ν is a smooth function of frequency (i.e., the Planck function) deep in the atmosphere where the monochromatic optical depth $\tau_\nu \gg 1$ for all frequencies, but J_ν obviously reflects the frequency variation of $\sigma(\nu)$ for $\tau_\nu \leq 1$. Therefore, the numerical representation of expression (48) has to be able to deal with the fact that the shape of J_ν varies significantly with depth. Likewise, the existence of two complicated functions with correlated frequency dependence precludes the use of any mean value representation of expression (48) using a simple mean of the cross section alone. In fact, the relevant mean value would be the *absorption* mean (Mihalas 1978), defined as

$$\bar{\sigma} = \frac{\int \sigma(\nu)J_\nu d\nu}{\int J_\nu d\nu} , \tag{49}$$

which is however not useful because J_ν is not known a priori. Another complication arises if there is another important opacity source in the interval (ν_0, ν_1) (e.g., a continuum edge, or another line/superline), so that J_ν reflects not only the variations of $\sigma(\nu)$, but also another, independent frequency variation. We shall return to this point in § 3.4.

An obvious possibility is to evaluate the integrals (48) straightforwardly by choosing a sufficient number of frequency points to represent all frequency variations of functions $f(\nu)$ and $\sigma(\nu)$. However, this would require thousands of points per superline, which is obviously out of the question. As discussed by Carbon (1984) in the context of LTE, or by Anderson (1989), in the context of non-LTE, one may use either the idea of opacity distribution functions (ODF), or a Monte Carlo–like sampling of frequency points. Both approaches suffer from certain drawbacks. The sampling technique generally requires a large number of frequency points, because the line cores which represent the regions of largest opacity are relatively narrow. Considering too few frequency points may easily lead to missing important line cores. Similarly, one may miss the regions of low opacity—the continuum "windows", where in fact most of the radiation flux is transported.

On the other hand, the idea of distribution functions is very attractive. The approach consists of resampling the cross section to yield a monotonic function of frequency and to represent this (monotonic) function by a relatively small number of frequency points. This procedure avoids all problems of missing opacities but suffers from another potentially serious problem of treating an overlap of two different distribution functions (cf. Carbon 1984)—see below. The idea of ODFs was first used in the non-LTE context by Anderson (1989), who nevertheless later (Anderson 1991) began to prefer the sampling technique. The sampling technique was also employed by Dreizler & Werner (1992, 1993).

A construction of the ODF is illustrated on the lower panel of Figure 2. First, the detailed cross section (the upper panel) is resampled to yield a monotonic function of frequency. For computational purposes, we are essentially free to choose whether this function will be monotonically decreasing or increasing with frequency, or whether it will be taken to be stepwise monotonic. We chose the following strategy: The peak of the ODF is placed at the position of the mean frequency of the individual superline components, weighted by the cross section, i.e., $\bar{\nu} = \int \nu\sigma(\nu)d\nu / \int \sigma(\nu)d\nu$. The ODF is then taken as a monotonically decreasing function in the direction toward the strongest individual line of the superline. In the case of Figure 2 this happens to be the direction of increasing wavelength (decreasing frequency). Once the real limit of the ODF is reached (i.e., $\lambda = 888$ Å in Fig. 2), the rest of the original resampled function is continued on the opposite side of the peak. In practice, we also select a certain criterion specifying the minimum value of the cross section considered; we use the value 10^{-7} of the maximum cross section (which is roughly analogous to considering a "normal" Doppler-broadened line from the core out to about 4 Doppler widths, which is a usual practice in model atmosphere calculations). Finally, we display in Figure 2 the frequency points which represent this ODF in model calculations — 24 points in this case.

The superline cross section, and consequently the ODF, generally depends on the depth in the atmosphere, through the dependence of the line broadening parameters on the temperature, density, and, to a lesser extent, on other state parameters. Instead of computing the exact ODF for every depth, or using an interpolation between two limiting values as suggested by Anderson (1989), we calculate the cross section and the ODF in three representative depths of the *actual atmosphere*; the first (surface) depth, the estimated depth of formation, and the last depth point. To obtain reasonably accurate ODFs for all depths, we simply interpolate (logarithmically) the set of representative ODFs in the *depth indices*. This procedure is quite adequate for the purposes of model construction. We plot in Figure 3 the ODFs for the transition displayed in Figure 2, for all three representative depths. The ODF remains almost unchanged between the surface (*dashed line*) and the approximate depth of formation (*full line*), while its shape is quite similar for the deepest depth point (*dot-dashed line*). The interpolation should not therefore produce significant errors, and even if so, the deep layers do not influence the formation of the spectrum because the monochromatic optical depth is already high.

From the general point of view, there are two basic problems connected with an application of ODFs. The first one concerns the inherent limitations of the statistical representation of the superline cross section, and the second one concerns the treatment of the superline overlaps.

The reliability of the distribution function representation rests on the following three assumptions. The first one, discussed in detail by Carbon (1984), is that the individual steps of the ODF histogram (i.e., an ODF represented by a stepwise function) are

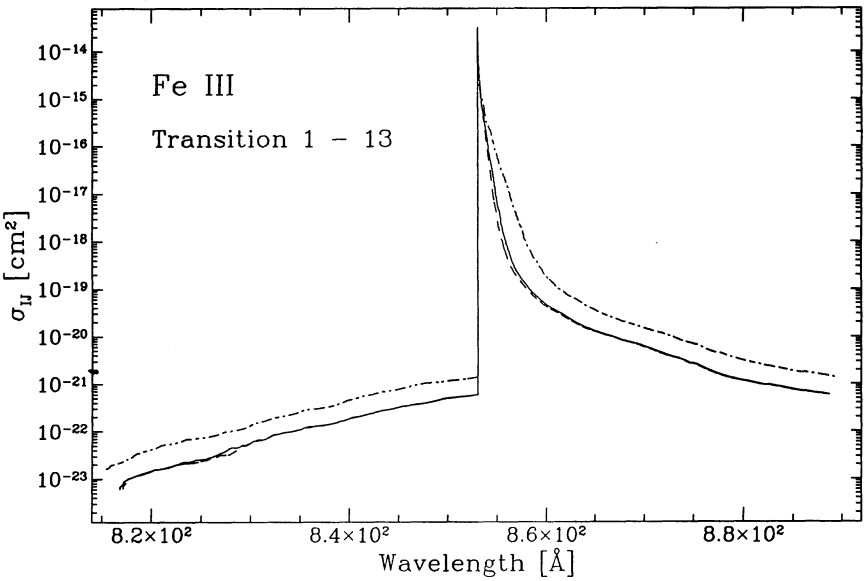

FIG. 3.—The ODFs for the same transition as displayed in Fig. 2, for the three representative depths: the first (uppermost) depth point, dashed line; the characteristic depth (the same as in Fig. 2), full line; the last (deepest) depth point, dot-dashed line

always identifiable with the opacity of particular frequency subintervals of the superline frequency range, at all depths in the atmosphere. In other words, the general shape of the detailed cross section has to be similar in all depths. The worst situation occurs if the cross section varies in such a way that a subinterval with high cross section at a certain depth becomes a subinterval with a small cross section at another depth. This problem may arise in the case where an ODF contains contributions from various species with different ionization degrees (such as in the traditional use of ODFs in LTE). Another important example is the treatment of differentially moving atmospheres, where a given frequency which corresponds to a line core at certain depth may be Doppler-shifted to correspond to a continuum window at a different depth. However, we consider here a static non-LTE atmosphere, and our ODFs represent the opacity of transitions arising between energy levels of nearly the same energy and of the same ion; therefore such problems never arise.

The second assumption is that if we construct the analogous distribution function for radiation intensity and represent it by the same histogram steps as the original ODF, then the particular frequency subintervals corresponding to the individual histogram steps must coincide with those corresponding to the cross section distribution function. In other words, both the cross section and the radiation intensity must have the same statistical distribution. This condition is not satisfied, for instance, if the radiation in the low–cross section part of the interval is both very low and very high; in other words, if the frequency variation of radiation field reflects not only the cross section of the given superline, but also of some other important, strongly frequency-dependent, opacity source.

The third, somewhat related, assumption is that the integrand $f(\nu)$ in expression (48) can be expressed as $f(\nu) = a(\nu)\sigma(\nu) + b(\nu)$, where $a(\nu)$ and $b(\nu)$ are smooth, nearly constant functions of frequency. However, both latter assumptions are never completely satisfied in reality. The problem is essentially the question of how to treat various overlaps. Since this is a very important and nontrivial problem, we will discuss it in detail in the next subsection.

3.4. *The Problem of Overlapping Transitions*

There are essentially three kinds of overlap which we will discuss in order of increasing complexity: (1) overlap of a superline with a strong bound-free discontinuity (continuum edge); (2) overlap of a superline with an ordinary spectral line; (3) overlap of two (or more) superlines.

1. Overlap of a superline with a continuum edge is very easy to deal with. It suffices to introduce two ODFs, instead of just one, to represent the corresponding superline. The first ODF represents the resampled opacity in the frequency interval (ν_0, ν_{edge}), while the second one spans the range (ν_{edge}, ν_1); ν_{edge} is the frequency of the continuum edge.

2. Overlap of a superline with an ordinary line is treated similarly. All we have to do is to represent the profile of the ordinary line by a histogram-like step function, and to construct an independent ODF for the individual frequency bins. The partitioning of the line into bins may be very simple; in fact as few as three bins—the line core region, the near wing region, and the wing region—may be adequate. We stress that in practice we do not have to use this procedure very often because the likelihood of significant overlap of a strong line (like, for instance, the hydrogen Lyα) and several strong metal lines is not very high. Overlap of weak individual lines within a given superline system with a strong ordinary line may be neglected.

3. Overlap of two superlines is, in principle, the most difficult situation to handle. It would be possible to use the same procedure as outlined above, i.e., to construct separate ODFs for an overlapped line for all frequency bins of the original superline ODF, but this would lead to an impractical number of ODFs. In some cases, this procedure may prove necessary, as for instance for treating the H I and He II high series member overlaps, because every other He II line of series $i \rightarrow n$ (with i even) significantly overlaps with a hydrogen line of series $i/2 \rightarrow n$. We shall consider this problem in a future paper.

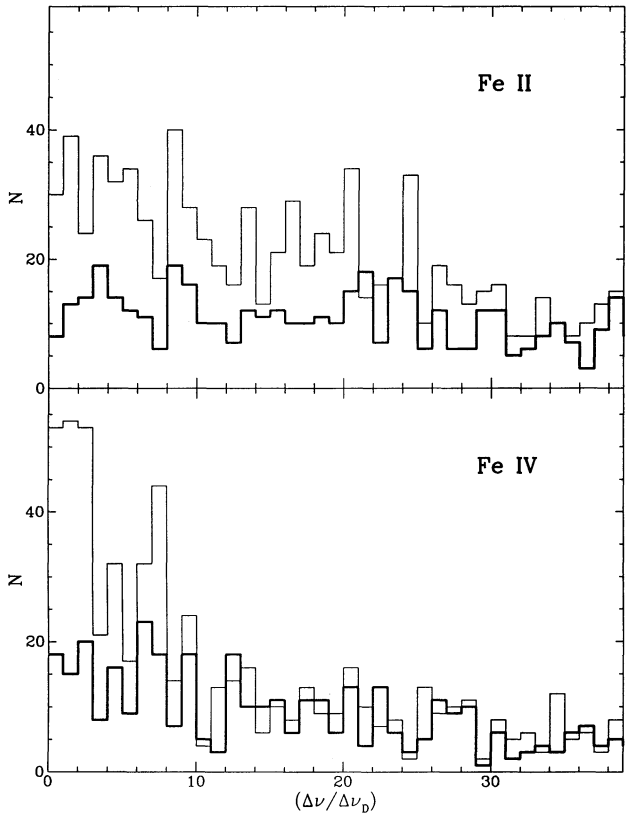

FIG. 4.—Histogram of distances between the individual "strong" spectral lines (defined by $\sigma_0 > 10^{-3}\sigma_0^{max}$) of the two selected ions of iron: upper panel, results for Fe II; lower panel, results for Fe IV; Thin line, all selected spectral lines are considered; heavy line, the spectral lines within the same superline are excluded. The abscissa represents the distance between the lines measured in units of the characteristic Doppler width, which is calculated for $T = 10{,}000$ K for Fe II, and $T = 30{,}000$ K for Fe IV. See the text and Table 6 for details

However, we claim that in most cases the overlap of superlines may be neglected. It should be clearly realized that although the *frequency regions* of the individual ODFs very often overlap, the true lines within different superlines overlap only very rarely. To demonstrate this point, we have analyzed the statistical distribution of distances between two neighboring lines, expressed in fiducial Doppler widths, for all "strong" lines of all interesting ions of iron (Fe II to Fe VI). We select the "strong" lines as those having the line-center cross section, σ_0, greater than a certain fraction of the maximum line-center cross section within the given ion, σ_0^{max}. We use here a criterion $\sigma_0 > 10^{-3}\sigma_0^{max}$. The fiducial Doppler width is calculated for a typical temperature at which the given ion is dominant. The results are presented in Figure 4 for two representative ions (Fe II and Fe IV), and in Table 6 for all ions. Figure 4 shows a histogram of distances, and Table 6 displays the percentage of lines which overlap within 1 and 4 fiducial Doppler widths. Only $\sim 10\%$ of lines overlap in the core (within 1 Doppler width); and typically 10%–20% of lines exhibit a core—near wing overlap (within 4 Doppler widths). However, a sizable fraction of these overlaps may in fact be overlaps of lines belonging to the same superline; and therefore such an overlap is treated essentially exactly by means of the ODF formalism. Figure 4 shows also the histogram of line distances, where the lines within the same superline were excluded (*thick lines*); and Table 6 displays corresponding

TABLE 6

PERCENTAGE OF OVERLAPPING IRON LINES

		Overlaps Within			
		Δv_D		$4 \times \Delta v_D$	
Ion	N_l[a]	1[b]	2[c]	1[b]	2[c]
Fe II	1449	2.1%	0.6%	8.9%	3.7%
Fe III	1378	4.6	1.7	15.5	5.7
Fe IV	765	8.0	2.4	23.7	6.9
Fe V	716	7.5	2.8	23.3	11.4
Fe VI	359	2.2	2.2	10.0	5.0

[a] Number of strong lines selected by $\sigma_0^i \geq 10^{-3}\sigma_0^{max}$.
[b] Overlaps between all considered lines.
[c] Overlaps between lines in different superlines.

percentages of lines that overlap within 1 and 4 fiducial Doppler widths. We see that indeed most of the overlaps are in fact overlaps of lines within the same superline, so that a substantial fraction of the total line overlap is treated essentially exactly.

This exercise shows that it is a very good approximation to neglect the overlap of different ODFs entirely. In practice, this is accomplished by selecting a set of frequency points describing all ODFs independently. Every superline has its own set of frequency points, and the total opacity in these points is calculated as a total continuum opacity (plus possibly a binned ordinary line opacity—see item [2]), and the opacity of the given superline. Although the frequency point distribution for several superlines may intersperse, the superlines "do not know about it" (and do not care).

3.5. *Frequency Quadratures*

As explained above, introducing separate sets of frequency points for continua and all lines (ODFs) offers a more flexible, and in fact physically more consistent, evaluation of opacity in the individual frequency points than simply sorting all frequencies in a monotonically decreasing (increasing) sequence, and assuming that all opacity sources (particularly ODFs) contribute in all frequencies. The drawback to our procedure is, however, that considerable care should be devoted to frequency integrations. In particular, one has to make sure that by having separate frequency points for continua and lines one does not integrate twice over the regions covered by lines. We use here a generalization of the procedure described by Hubeny (1988, § 5.2).

Let us evaluate an integral $\int_0^\infty F(\nu)d\nu$ (function F may vanish for any subinterval). Let us further assume that function F is essentially "smooth" for most of the total frequency range (continuum), while it exhibits a sharp variation in one or more narrow frequency intervals (lines). We divide the frequency quadrature into three parts. First, we integrate over the "continuum points," which are selected to describe accurately the "continuum" (including all continuum edges, but possibly also wide, e.g., hydrogen, lines). Second, for each "line," we have to subtract the partial integral of the "continuum" part of function F over the region covered by the line. The third contribution is the numerical integration over the "line" frequency points. Denoting as IFR0(IT) and IFR1(IT) the indices of the first and last frequency point within the line IT, we may express the general frequency quadrature as

$$\int_0^\infty F(\nu)d\nu = \sum_{i=1}^{\mathrm{NFREQC}} F(\nu_i)w_i + \sum_{\mathrm{IT}=1}^{\mathrm{NLINE}} \left[-\sum_{\mathrm{IFRC0(IT)}}^{\mathrm{IFRC1(IT)}} F(\nu_i)w_i^{\mathrm{sub}} + \sum_{\mathrm{IFR0(IT)}}^{\mathrm{IFR1(IT)}} F(\nu_i)w_i \right], \tag{50}$$

where NFREQC is the total number of continuum frequency points, w_i are the original frequency quadrature weights, and NLINE is the total number of lines, including superlines.

To evaluate the "subtraction integral"—the second term of equation (50)—we may use a simple procedure described by Hubeny (1988), viz.,

$$I^{\mathrm{sub}} = F(\nu_{\mathrm{last}})\Delta\nu_{\mathrm{line}}\,, \tag{51}$$

where ν_{last} is the last frequency point within the line (where the influence of the line is negligible) and $\Delta\nu_{\mathrm{line}}$ is the total frequency range covered by the line. Equation (51) is a satisfactory approximation in the case of a narrow line. However, in the present case, the lines, and particularly the superlines, may be rather wide, and the above approximation would be quite inaccurate. To evaluate an improved subtraction integral, we first find all subintervals of the original "continuum" frequency quadrature which overlap the frequency range of the given line IT. We denote the corresponding limiting indices as IFRC0(IT) and IFRC1(IT). The frequency integration over continuum consists of a set of simple numerical quadratures, the trapezoidal or the Simpson integrations. Integrating function $F(\nu)$ in fact means to integrate analytically a set of polynomials $P(\nu)$ of the first degree (in the case of trapezoidal integration) or the second degree (in the case of Simpson integration), such as $P(\nu_i) = F(\nu_i)$ for all continuum points ν_i. Thus, the result depends only on values of $F(\nu)$ in the continuum frequency quadrature points, and on the minimum and maximum frequency points within the line. The subtraction integral is therefore given by

$$I^{\mathrm{sub}} = \int_{\Delta\nu} P(\nu)d\nu = \sum_{\mathrm{IFRC0(IT)}}^{\mathrm{IFRC1(IT)}} F(\nu_i)w_i^{\mathrm{sub}}\,, \tag{52}$$

where the "subtraction" weights w_i^{sub} depend only on the continuum frequencies ν_i, $i = \mathrm{IFRC0(IT)}, \ldots, \mathrm{IFRC1(IT)}$, and the minimum and maximum frequency within the line, ν_0 and ν_1.

4. ILLUSTRATIVE MODEL CALCULATIONS

We will address two separate issues here. First, we will test the performance of the hybrid CL/ALI method. To this end, we choose a relatively simple model which allows us to explore the whole range of options for the frequency point partitioning between the CL and ALI method. Second, we will present two representative models with non-LTE line blanketing of iron, one for $T_{\mathrm{eff}} = 21{,}000$ K; $\log g = 3.2$, corresponding to an early B giant (in fact, this model represents our model atmosphere for ϵ CMa—see Cassinelli et al. 1995), where blanketing by Fe III and Fe IV lines is important, and the other for $T_{\mathrm{eff}} = 55{,}000$ K; $\log g = 5.3$, representing a typical sdO star, where blanketing by Fe IV, Fe V, and Fe VI is most important. We do not present here models for A or late B stars where the Fe II line blanketing is dominant because some illustrative model results were presented earlier (Hubeny & Lanz 1993a). Other preliminary results obtained by the present method can be found in Lanz et al. (1992)—for relatively cool ($T_{\mathrm{eff}} \simeq 15{,}000$ K) metal-rich white dwarfs found in some cataclysmic variable systems; Heap et al. (1992)—for hot O subdwarfs; and Hubeny & Lanz (1993b)—for hot, metal-rich white dwarfs.

4.1. *Performance of the Hybrid Method*

We have selected a H-He model atmosphere for $T_{\mathrm{eff}} = 25{,}000$ K; $\log g = 4$, $N(\mathrm{He})/N(\mathrm{H}) = 0.1$, which represents an early B main-sequence star. For hydrogen, the eight lowest levels are considered explicitly, while all the higher states are treated as a

"merged level," adopting an occupation probability treatment of their dissolution, as described in Hubeny et al. (1994). The treatment of hydrogen is thus essentially exact. He I is represented as a 15 level atom; all *ls*-states up to $n = 2$ are treated as separate levels; levels with $n = 3, 4, 5$ are treated by averaging separately the singlet and the triplet states, and the higher levels up to $n = 8$ are averaged over all *ls*-states within each *n*. H II and He II are represented by one-level ions. The continuum is represented by 79 frequency points, which provides a reasonably accurate numerical frequency quadrature.

The model atmosphere calculation proceeds, as usual, in three steps. First, an LTE model is calculated starting from an LTE-gray model. The next step is a NLTE/C (continuum only) model, where all lines are assumed to be in detailed radiative balance. The final step is a NLTE/L, where in addition some or all lines are considered explicitly. In some case, it is in fact possible to skip one of the first two steps. For instance, it may be possible to proceed from the converged LTE model directly to NLTE/L; sometimes it is easier to proceed from the LTE-gray model directly to NLTE/C, rather than to converge an LTE model (as, for instance, in the case of heavily line-blanketed model). Nevertheless, in the present paper, we will consider the models calculated in all three steps.

All the following models were calculated on a DEC 3000/400 (Alpha) workstation running under a Unix-based operation system, OSF/1. All timing comparisons reported here refer to runs of the program on this workstation.

4.1.1. *LTE Models*

The ALI method was not originally intended to be used in the context of LTE, but it is perfectly legitimate to do so. Although the statistical equilibrium equations are replaced by the Saha-Boltzmann formulae, and therefore the level populations do not have to be solved for, the remaining radiative and hydrostatic equilibrium equations still contain the unknown radiation intensity explicitly. As a consequence, when applying the standard CL, where one explicitly linearizes the radiation intensity, computing LTE models is roughly as time-consuming as computing NLTE/C models. To provide a fair performance test, which could be used to estimate the computer time demands in actual model calculations, we employ our previously developed acceleration schemes (Hubeny & Lanz 1992), namely the Kantorovich and Ng acceleration. A model is declared converged if the maximum relative change of all quantities at all depths, $\delta\psi_{\max}$, is less than 10^{-3}.

Table 7 summarizes the computed LTE models. Convergence properties of the individual models are presented in Figure 5*a*, where the maximum relative change is plotted as a function of the iteration number. Model A represents the standard (accelerated) complete linearization, where all frequency points are linearized. Ng acceleration is started at seventh iteration and performed every four iterations, and the Kantorovich acceleration is started at the third iteration. Model B represents the opposite extreme, namely a pure ALI scheme. We use the same setup for the Ng acceleration as before. If the Kantorovich acceleration is started after the third iteration as for the standard CL, the convergence is relatively slow. However, when the Kantorovich acceleration is switched on after eighth iteration (as was done in model B), the convergence is more uniform. We shall return to this point later. Model C considers 10 frequencies as explicit, and the rest (69) as ALI. The 10 explicit frequencies are chosen to be the first five points (with lowest frequencies) in the Lyman and Balmer continua. Finally, model D considers only two points as explicit (the first two points in the Lyman continuum). In both latter models, the Kantorovich acceleration is switched on after the fourth iteration.

The most interesting result is that considering as few as two points to be explicit (linearized) dramatically increases the convergence rate (i.e., decreases the number of iterations to achieve a required accuracy) with respect to the standard ALI, while the time per iteration remains virtually the same. This clearly shows the superior properties of the hybrid scheme over both the pure ALI scheme and the pure CL method. We have verified that the resulting models are indeed well converged; for instance, the maximum temperature difference between models A, B, C, and D was found to be about 0.7 K.

To display the favorable timing properties of the hybrid scheme, we plot in Figure 5*b* the maximum relative change as a function of the total CPU time at the end of every iteration step (including formal solution). It is clearly seen that although the standard CL has the highest convergence rate, the total time is much larger than for the other methods (a sharp turnover of the curve for model A at the third iteration corresponds to the onset of Kantorovich acceleration). And, most importantly, the hybrid scheme (model D) takes only about 60% of the computer time as for the full ALI scheme (model B).

To study the effects of Ng and Kantorovich accelerations on the convergence properties of the full ALI scheme, we have calculated several additional models, denoted B1, B2, B3, and B4—see Table 7 and Figure 6. Model B1 is identical to model B discussed previously. Models B1 and B2 apply the Ng acceleration, started after the seventh iteration, and performed every four iterations. The Kantorovich variant is started after the eighth and the third iteration for models B1 and B2, respectively. Analo-

TABLE 7

CHARACTERISTICS OF LTE MODELS

MODEL	FREQUENCIES EXP	FREQUENCIES ALI	START KANTOROVICH	$N_{\rm ITER}$	$t_{\rm CPU}$ (s)
A.....	79	0	3	7	106
B.....	0	79	8	19	67
C.....	10	69	4	11	47
D	2	77	4	10	40
B1	0	79	8	15	64
B2	0	79	3	23	74
B3[a].....	0	79	8	27	87
B4[a].....	0	79	3	27	76

[a] No Ng acceleration.

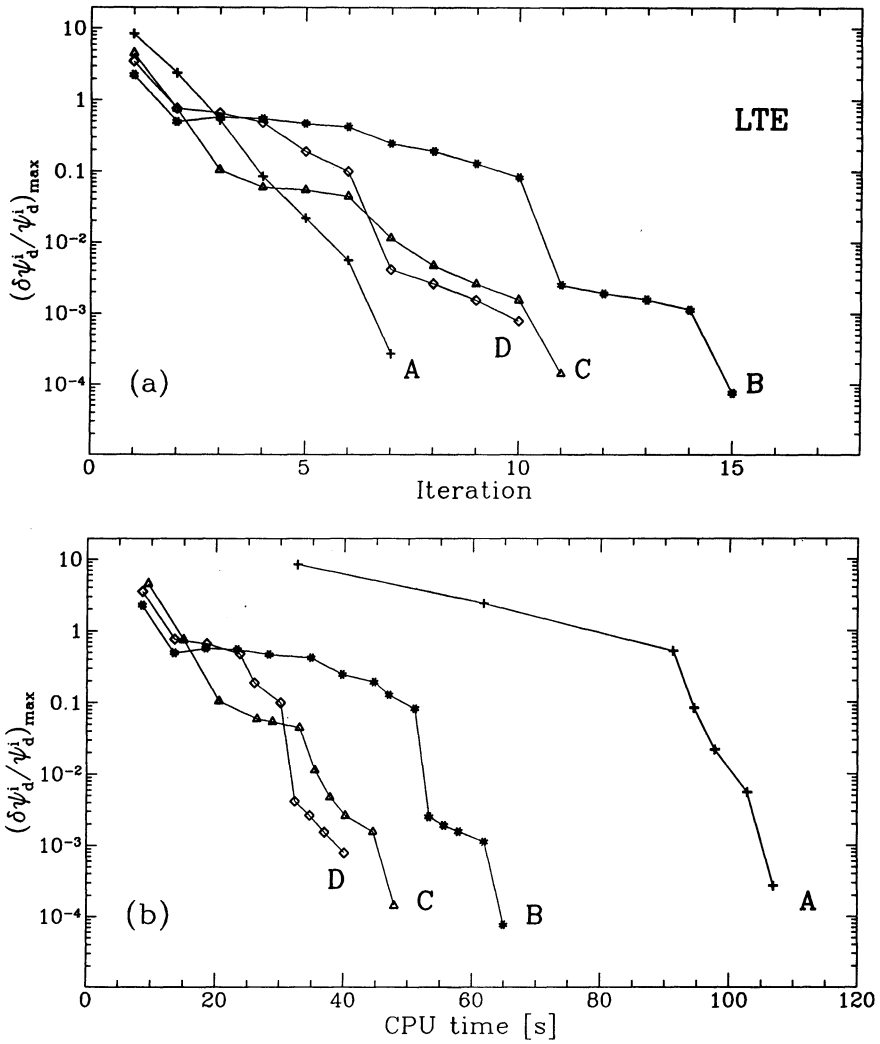

FIG. 5.—Convergence properties of the individual LTE models for our standard test case atmosphere: a H-He model with $T_{\rm eff} = 25{,}000$ K; $\log g = 4$ (see Table 7) (*a*) The maximum relative change is plotted as a function of the iteration number; (*b*) The maximum relative change as a plotted as a function of the total CPU time at the end of every iteration step (including formal solution). Model A, the standard (accelerated) complete linearization; model B, pure ALI scheme; model C, hybrid scheme (10/69—i.e., 10 points explicit; 69 ALI); model D, hybrid scheme (2/77).

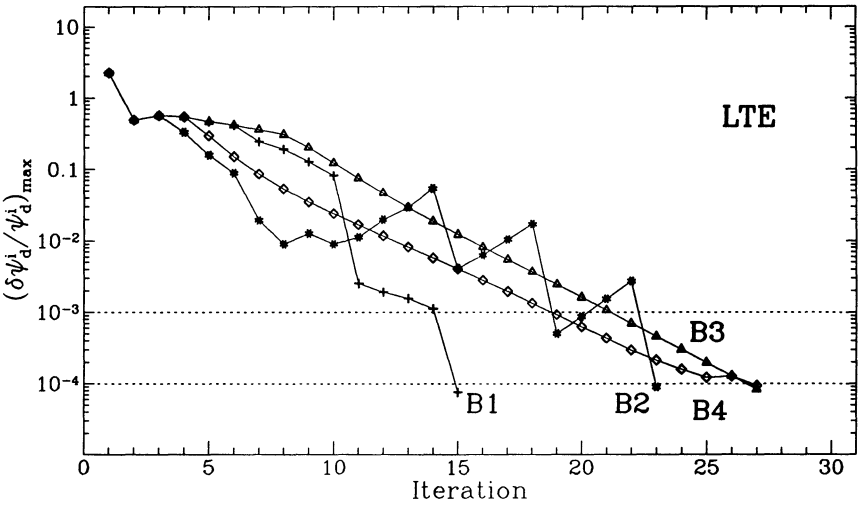

FIG. 6.—Effect of the Kantorovich and Ng acceleration on convergence properties of LTE models calculated by the full ALI scheme (see Table 7). Model B1, Ng acceleration (started at seventh iteration, performed every four iterations), Kantorovich acceleration (started at eighth iteration); Model B2, Ng (7/4); Kantorovich (3); model B3, no Ng, Kantorovich (8); model B4, no Ng, Kantorovich (3). Dotted horizontal lines at 10^{-3} and 10^{-4} indicate the two adopted convergence criteria

gously, models B3 and B4 do not apply Ng acceleration at all, while the Kantorovich variant is again switched on after the eighth and third iteration, respectively. The maximum relative change to declare convergence was now decreased to $\delta\psi_{\max} < 10^{-4}$. The convergence of the ALI scheme without Ng acceleration is rather monotonic, but relatively slow. Ng acceleration provides much better convergence; however, if the Kantorovich variant is switched on too soon (B2), the convergence is rather bumpy. This is because the Jacobi matrix, being fixed after the third iteration, is still very far from the exact Jacobi matrix of the system (Hubeny & Lanz 1992).

Finally, we stress that the present case still does not show the advantage of the hybrid scheme in full, because the number of frequency points we consider here is rather low. In more realistic and/or accurate models, where the number of frequency points in the continuum has to be of the order of several hundreds, we always find the analogous behavior: When only a few frequency points are linearized, the time per iteration is the same, but the convergence rate is much faster than in the case of pure ALI, and the total computer time is orders of magnitude shorter than for the standard CL. This point is nicely illustrated in non-LTE models with lines, considered in § 4.1.3.

4.1.2. *NLTE/C Models*

Again, we calculate four models, denoted A, B, C, D, analogous to the case of LTE (see Table 8). The results are very similar to those for LTE models. Nevertheless, when we choose the same convergence criterion as for the LTE models, $\delta\psi_{\max} < 10^{-3}$, we find that the maximum temperature difference between models is about 11 K. This is certainly negligible for any astrophysical application, but since we are exploring here the numerical properties of various schemes, we have to verify that all methods would eventually converge to the same results. When we change the convergence criterion to $\delta\psi_{\max} < 10^{-4}$, the maximum temperature difference between resulting models decreases to about 2 K. The convergence properties and timing are displayed in Figures 7*a* and 7*b*, where we indicate the two convergence criteria by dotted horizontal lines.

Standard CL (model A) again converges very fast (in seven iterations). The full ALI scheme with the Kantorovich and Ng accelerations (model B) converges at first rather quickly, but later slows down. The original criterion, $\delta\psi_{\max} < 10^{-3}$, was reached in nine iterations, while it took another 10 iterations to decrease $\delta\psi_{\max}$ by an order of magnitude. The hybrid scheme (models C and D) again provides a significant improvement. Using the original convergence criterion, model C (10 points explicit, 69 points ALI) converges at even a greater rate than the standard CL according to the original criterion (in six iterations), and it needed only three additional iterations to reach the more accurate convergence criterion. Nevertheless, the gain in total computer time is significant (see Fig. 7*b*). Model D (two points explicit) now converges slightly slower than model C; the total time is only marginally longer for the original convergence criterion (49 s as compared to 45 s for C), while the difference is larger (72 s vs. 54 s) for the more accurate convergence criterion.

Finally, to show the full range of improvements of the complete linearization method developed here and in the previous paper (Hubeny & Lanz 1992), we have calculated one more model, A0 (see Table 8), using the original (unaccelerated) CL. We plot the timing in Figure 8. The plot dramatically shows the improvement of the original CL due to the Kantorovich acceleration (a sharp turnover of curve A at the third iteration), which yields a factor of two of acceleration in this case and another substantial time gain due to the hybrid scheme (model C).

4.1.3. *NLTE/L Models*

As explained above, we intend to test the whole possible range of frequency point partitioning. Therefore, we chose to calculate a simplified model where all He I lines are kept in detailed radiative balance, while only hydgrogen lines are treated explicitly. The model where all He I lines are also allowed explicitly would be easy to calculate by the hybrid scheme, but it would take an impractically large computer time in case all frequency points are treated explicitly. In fact, such models (although still much more complicated) are considered in § 4.2; a comparison to the standard CL would be meaningless because CL would require several tens to hundreds hours of computer time.

In the present models, we assume a depth-independent Doppler profile, with five frequency points per line. The line profile is assumed symmetric about the line center so that only one half of the profile is considered; frequency points are spaced equidistantly between the line center and the wing at four fiducial Doppler widths (defined as the Doppler width at $T = 0.75 \times T_{\rm eff}$). All lines between the first eight levels of hydrogen are considered, which gives 28 "normal" lines. Next, we consider two superlines which represent the higher members of the Lyman and Balmer series, as described by Hubeny et al. (1994). The superlines are represented by 14 and 16 frequency points, respectively. Altogether, we use 170 line frequency points, which results in a total of 249 frequency points.

TABLE 8

CHARACTERISTICS OF NLTE/C MODELS

MODEL	FREQUENCIES EXP	FREQUENCIES ALI	START KANTOROVICH	$N_{\rm ITER}$	$t_{\rm CPU}$ (s)
A.....	79	0	3	7	122
B.....	0	79	4	19	97
C.....	10	69	4	8	54
D.....	2	77	4	13	72
A0[a].....	79	0	...	7	234

[a] No Kantorovich and Ng accelerations.

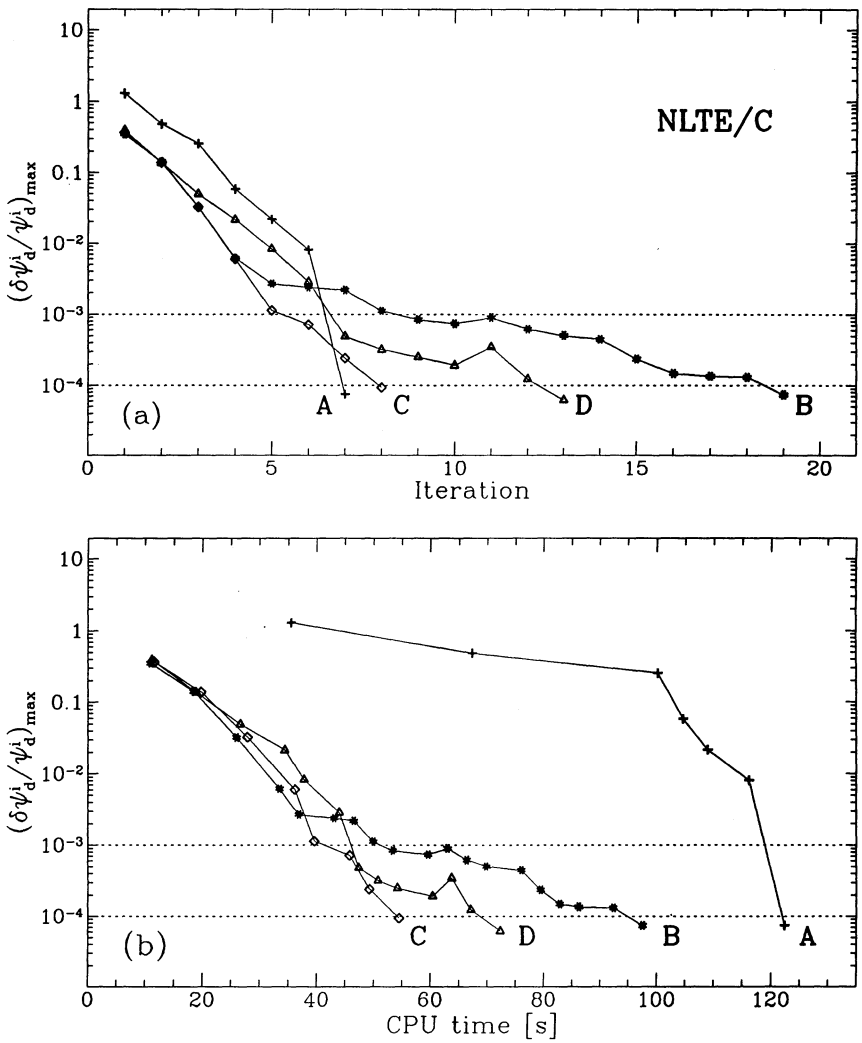

FIG. 7.—Convergence properties of the individual NLTE/C models for our standard test case atmosphere (see Table 8). (*a*) The maximum relative change is plotted as a function of the iteration number; (*b*) the maximum relative change is plotted as a function of the total CPU time at the end of every iteration step. Model A, the standard (accelerated) CL; Model B, pure ALI scheme; Model C, hybrid scheme (10/69); model D, hybrid scheme (2/77)

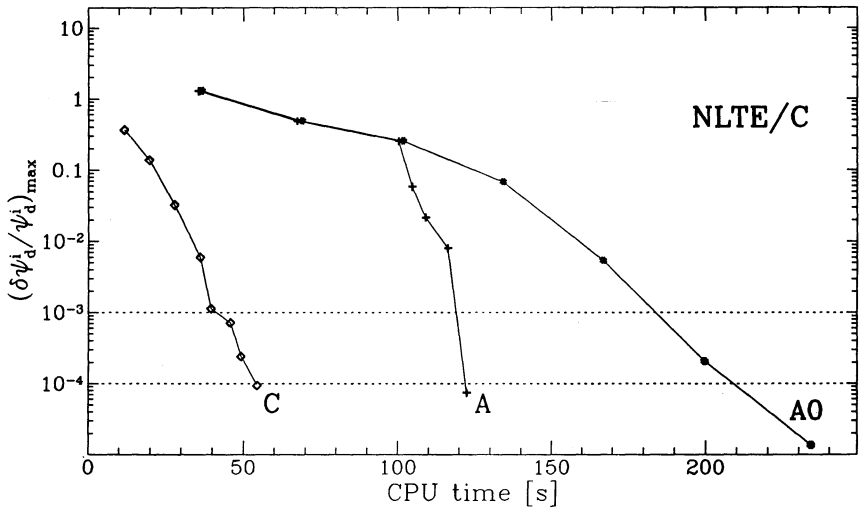

FIG. 8.—A comparison of the timing for NLTE/C models for the standard test case atmosphere. Model A0, unaccelerated CL; model A, accelerated CL; and model C, the hybrid scheme. The plot is analogous to Fig. 7*b* and shows the dramatic improvement of the complete linearization method achieved in the last two years

TABLE 9

CHARACTERISTICS OF NLTE/L MODELS

MODEL	FREQUENCIES EXP	FREQUENCIES ALI	START KANTOROVICH	N_{ITER}	t_{CPU} (s)
A.....	249	0	3	11	2658
B.....	0	249	4	40	384
C.....	4 + 30	215	4	11	181
D.....	4 + 8	237	4	13	178
A0[a].....	249	0	...	7	5307

[a] No Kantorovich and Ng accelerations.

All models are calculated with the Ng acceleration started at the seventh iteration and performed every four iterations, and with the Kantorovich variant started at the third iteration for model A, and the fourth iteration for other models. Model A again represents the standard CL scheme. Model B is the full ALI scheme, and models C and D represent two setups of the hybrid scheme. In both later models, we have selected four frequencies in the continuum as explicit (the first four points in the Lyman continuum). Model C sets all points in the Lyα, Lyβ, Lyγ, Hα, Hβ, and Paα lines as explicit, while all points in the remaining 22 normal lines and two superlines are ALI; model D takes only eight line frequency points as explicit, namely the two frequencies closest to the line core for Lyα, Lyβ, Lyγ, and Hα—see Table 9.

When the convergence criterion $\delta\psi_{max} < 10^{-3}$ was applied, the maximum temperature difference between model A and B was about 20 K at $\log m \approx -2$ (the continuum-forming layer), while it reached about 220 K at the surface. Again, although these differences are likely of little practical consequence, we decided to choose a more stringent convergence criterion, $\delta\psi_{max} < 10^{-4}$, to study in detail the convergence properties of all adopted numerical procedures. Figures 9*a* and 9*b* show the convergence properties and timing. As expected, the standard (accelerated) CL has a fast convergence rate, but the time per iteration is very large—*any variant of the hybrid scheme, including the full ALI, provides a fully converged model long before the first iteration of the CL method is completed*! When the lower accuracy convergence criterion was used, the full ALI scheme (model B) required only slightly more computer time (about 20%–25%) than the models computed using the hybrid scheme (models C and D). However, to obtain the converged model according to the higher accuracy criterion, the hybrid scheme required only about half of the computer time of the full ALI scheme.

Again, to display the full range of improvement of the CL method, we have calculated model A0, as described in the previous subsection, using the original (unaccelerated) CL. We plot the timing in Figure 10. The CPU time differences between the individual methods are now so large that we have to use a logarithmic scale on the time axis! There is a factor of two improvement in timing between the original CL (model A0) and the accelerated one (A); another factor of 7 between the accelerated CL and the original ALI (model B), and finally factor of 2 between the pure ALI and the hybrid scheme (model D), so altogether we gain a factor of 30 of acceleration!

Finally, we stress that the hybrid scheme is preferable to the full ALI method not only because it is faster, but also, and perhaps more importantly, because it is significantly more accurate. We plot in Figure 11 the temperature difference between model A (presumably "exact"), and the remaining models B, C, and D. While models C and D are now within 2 K from the exact model, model B (full ALI) still exhibits a difference of about 40 K high in the atmosphere. Notice that this difference is significantly larger than the "expected" difference $10^{-4}T$, in virtue of the adopted convergence criterion, which would amount to about 2 K. The reason is that ALI converges very slowly, so that small values of relative changes do not necessarily guarantee a fully converged solution. We will return to this point in § 5, but the basic conclusion of this section is that the hybrid CL/ALI scheme appears to be the most advantageous variant of the ALI method to be used for model atmosphere calculations.

4.2. *Examples of Non-LTE Line-blanketed Model Atmospheres*

4.2.1. *An Early B Star:* $T_{eff} = 21{,}000$ K; $\log g = 3.2$

First, we calculate several model atmospheres for $T_{eff} = 21{,}000$ K; $\log g = 3.2$—see Table 10. The atmosphere is assumed to be composed of hydrogen, helium, and iron, with $N(\mathrm{He})/N(\mathrm{H}) = 0.1$, and $N(\mathrm{Fe})/N(\mathrm{H}) = 2.5 \times 10^{-5}$ (i.e., the solar abundances). The treatment of hydrogen and helium is exactly the same as for the models considered in the previous subsection, except that now we also consider in certain models all the allowed transitions in He I between the levels with n up to $n = 8$. For iron, we consider four ionization degrees; Fe II and Fe V are represented by one-level ions (Fe II is considered for completeness since in the temperature minimum region its population is nonnegligible, while Fe V represents the highest ionization degree). As described above (§ 3.1; Table 2), Fe III is represented by 27 superlevels and 191 superlines which in turn represent 23,059 genuine lines (all lines originating between the levels with measured energies). Fe IV is represented by 21 superlevels and 109 superlines, which similarly represent 7897 genuine lines.

Model 1 is a simple H-He NLTE/C model, i.e., a model where all lines are put in detailed radiative balance. Model 2 is a classical H-He NLTE/L model, i.e., with all lines of hydrogen and He I considered explicitly. Models 3, 4, 5 include iron; model 3 considers all lines of Fe IV explicitly, but all other lines (i.e., of H, He, and Fe III) are in detailed radiative balance. Model 4 considers all lines of Fe III and Fe IV explicitly, but no lines of H and He. Finally, model 5 considers all lines of H, He I, Fe III, and Fe IV. This last model is calculated using 7777 frequency points; 735 in continua, and the rest in lines. Out of this number, 17 points in continuum and 28 points in lines were linearized. These numbers represent a conservative choice; it is quite possible that we could have chosen fewer

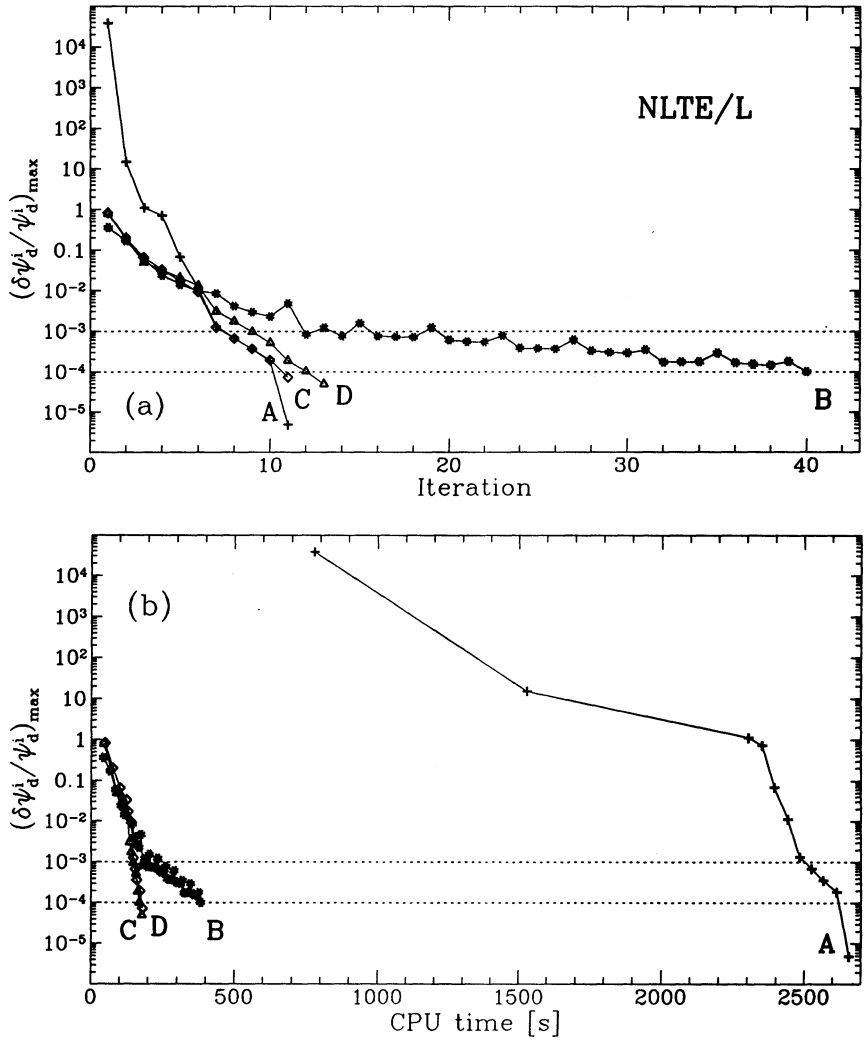

FIG. 9.—Convergence properties of the individual NLTE/L models for the standard test case atmosphere (Table 9). (*a*) The maximum relative change is plotted as a function of the iteration number; (*b*) the maximum relative change is plotted as a function of the total CPU time at the end of every iteration step. Model A, the standard (accelerated) CL; Model B, pure ALI scheme, Model C, hybrid scheme (32/215); Model D, hybrid scheme (12/235)

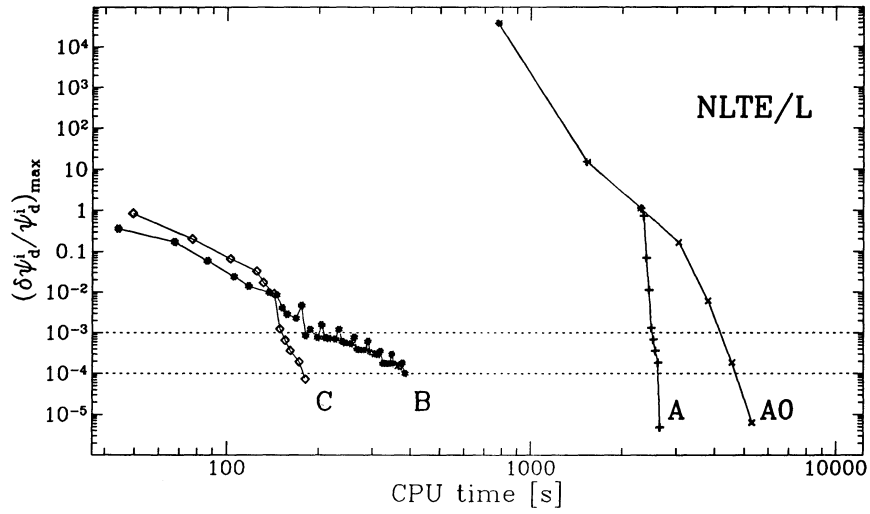

FIG. 10.—A comparison of the timing for NLTE/L models for the standard test case atmosphere. Model A0, unaccelerated CL; model A, accelerated CL, model B, pure ALI scheme; and model C, the hybrid scheme. The plot is analogous to Fig. 9*b* and shows the full range of recent improvement of the complete linearization method. Notice the logarithmic scale on the time axis

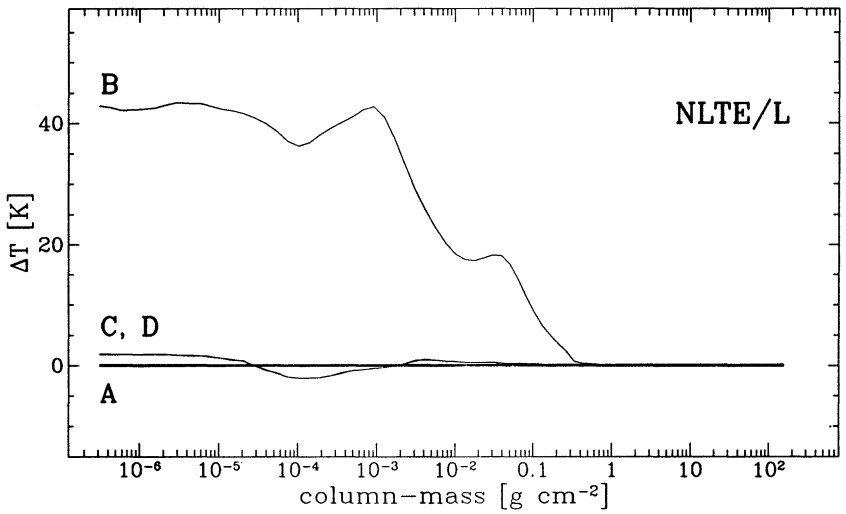

FIG. 11.—Temperature difference (in K) between the NLTE/L model A ("exact"), and models B, C, and D displayed in Fig. 9. Notice that while model B (computed by the ALI scheme) was declared converged, there is still a difference from the exact model of about 40 K at the surface. The models calculated by the hybrid scheme (C and D) are both within 2 K from the exact model

points to be linearized, but since the model calculations are rather time-consuming, we did not make any effort to optimize the choice at this stage.

Figure 12 displays the run of temperature versus the column mass for all five models. The temperature rise for $\log m < -2$ for model 2 is a classical non-LTE effect first discovered by Auer & Mihalas (1969) and is explained as an indirect effect of Balmer lines on the heating rate in the Balmer continuum. The temperature decrease at $\log m < -4$ represents the cooling effect of the hydrogen Lyman lines and the He I resonance lines. When only the Fe IV lines are allowed for, we obtain a mild backwarming effect (a temperature increase for $\log m > -2$), and an appreciable surface cooling. When also Fe III lines are allowed for, both effects are considerably enhanced because Fe III provides much more line opacity than Fe IV in this temperature range. Also, there are many more lines of Fe III in the UV spectral range where the flux is maximum. When all lines are allowed for (model 5), the temperature is much lower than for the H-He NLTE/L model (model 2) for $\log m < -2.5$ (due to the surface cooling produced by iron lines), while it is higher elsewhere (the backwarming effect). These results show that line blanketing is indeed very important in the atmospheres of B stars. A more detailed discussion of the non-LTE model atmosphere, and a comparison to the observed spectrum of ϵ CMa in the EUV, UV, visible, and IR ranges is presented by Cassinelli et al. (1995).

Finally, we plot in Figure 13 the emergent flux for model 5 in the frequency points considered in the model construction. We stress that this is not a synthetic spectrum; all these points are indeed fully considered in the linearization (explicitly or by means of ALI).

4.2.2. *A Hot Subdwarf:* $T_{\rm eff} = 55{,}000$ K; $\log g = 5.3$

Next, we calculate several model atmospheres for $T_{\rm eff} = 55{,}000$ K; $\log g = 5.3$—see Table 11. The atmosphere is assumed to be composed of hydrogen, helium, carbon, nitrogen, oxygen, and iron; with $N({\rm He})/N({\rm H}) = 1.5$, $N({\rm C})/N({\rm H}) = 9.2 \times 10^{-5}$, $N({\rm N})/N({\rm H}) = 6.3 \times 10^{-3}$, $N({\rm O})/N({\rm H}) = 1.7 \times 10^{-4}$, and $N({\rm Fe})/N({\rm H}) = 1.2 \times 10^{-4}$. This chemical composition and the basic parameters roughly mimic a mildly helium-rich, hot O subdwarf, such as for instance BD +75°325.

The treatment of hydrogen is the same as before. He I and He III are represented by one-level atoms; while He II is represented by a 14-level ion. For carbon we consider explicitly one level for C III, 12 levels for C IV, and one level for C V. Similarly, for nitrogen, we consider one level of N III, six levels of N IV, nine levels of N V, and one level of N VI. For oxygen, we consider a simplified model

TABLE 10

NUMBER OF NON-LTE LEVELS, LINES AND SUPERLINES, AND FREQUENCIES INCLUDED IN THE MODEL ATMOSPHERES WITH $T_{\rm eff} = 21000$ K, $\log g = 3.2$

	NON-LTE LEVELS[a]		LINES		FREQUENCIES		
MODEL	H, He	Fe	Model[b]	Actual[b]	EXP	ALI	Total
1	25	0	0	0	8	71	79
2	25	0	90	232	45	1330	1375
3	25	50	119	7917	29	2672	2701
4	25	50	312	30976	29	6344	6373
5	25	50	402	31188	45	7732	7777

[a] Individual levels or superlevels (H I merged higher states, iron superlevels).
[b] Number of lines or superlines in the models; the number of genuine atomic lines included in the models are given in the next column

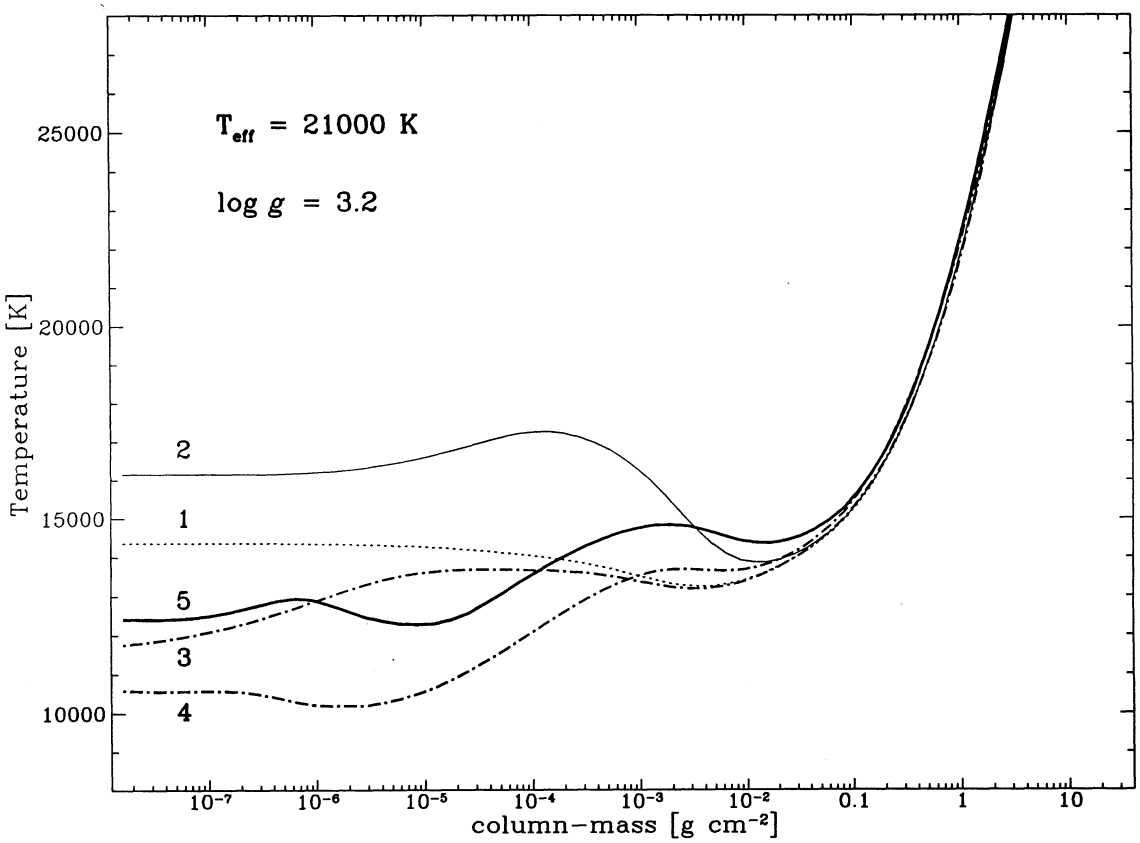

FIG. 12.—Plot of the temperature vs. column mass for various model atmospheres with $T_{\rm eff}$ = 21,000 K; log g = 3.2 (a typical early B giant: Table 10). Model 1, simple H-He NLTE/C model (no lines considered); model 2, He-He NLTE/L model (all lines of H and He considered); model 3, H-He-Fe model, only Fe IV lines considered; model 4, H-He-Fe model, Fe III and Fe IV lines considered; model 5, H-He-Fe model, all lines (H, He, Fe III, and Fe IV) considered.

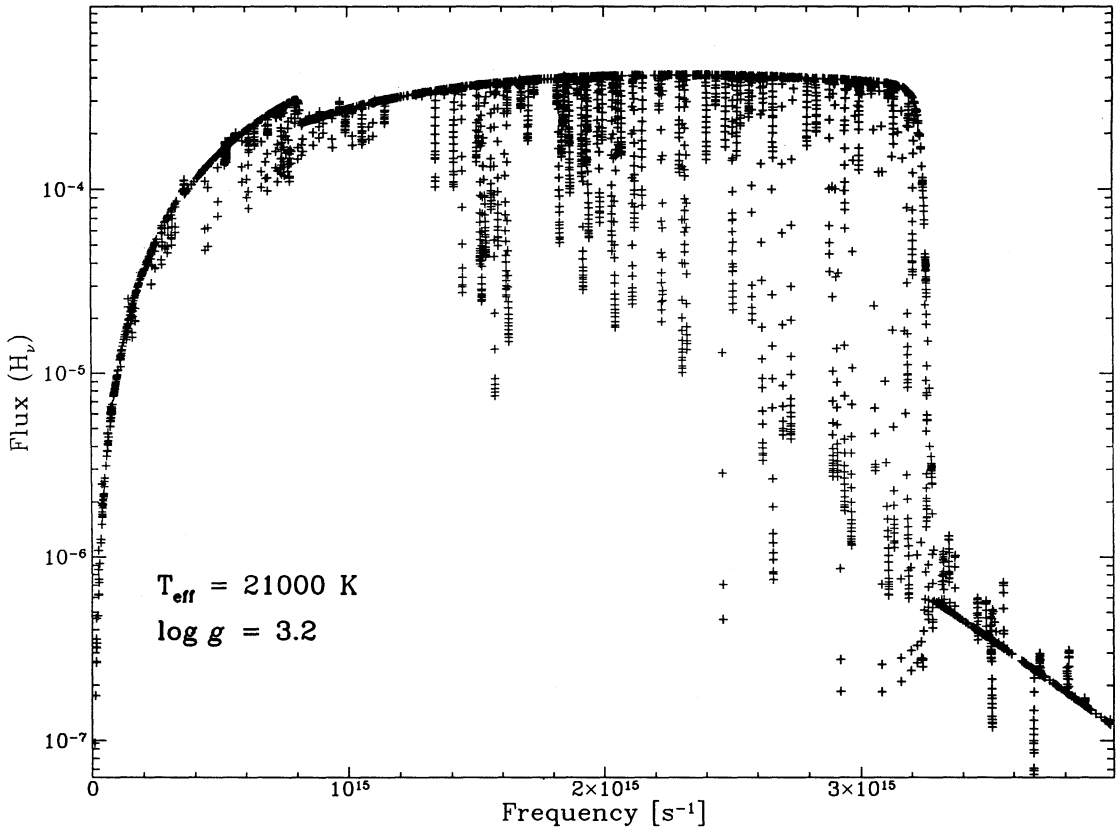

FIG. 13.—Emergent flux for the H-He-Fe line-blanketed model atmosphere for $T_{\rm eff}$ = 21,000 K; log g = 3.2 (model 5 of Fig. 12). The plot does *not* represent the synthetic spectrum; it displays the flux at the frequency points which were explicitly used in the model construction (7777 points altogether)

TABLE 11

NUMBER OF NON-LTE LEVELS, LINES AND SUPERLINES, AND FREQUENCIES INCLUDED IN THE MODEL ATMOSPHERES WITH T_{eff} = 55,000 K, log g = 5.3[a]

	NON-LTE LEVELS			LINES		FREQUENCIES		
MODEL	H, He	C, N, O	Fe	Model	Actual	EXP	ALI	Total
1	26	0	0	0	0	9	636	645
2	26	0	0	121	263	23	1479	1502
3	26	39	0	165	307	25	1785	1810
4	26	39	52	396	12974	25	6125	6150

[a] Columns are analogous to those in Table 10.

consisting of one level for O III and O IV, five levels for O V, and one level for O VI. We stress that these simple models are chosen for illustration purposes only; for a detailed spectroscopic study of hot subdwarfs, much more complete model atoms should be used. Finally, four ionization stages of iron are considered. Fe IV is treated as before (21 superlevels); Fe V is represented by 19 superlevels and 82 superlines, which represent 3670 genuine lines; Fe VI is represented by 11 superlevels and 31 superlines, which similarly represent 1100 genuine lines. Fe VII is considered as a one-level ion.

We have calculated several model atmospheres with increasing number of lines considered—see Table 11. Model 1 is a simple H-He NLTE/C model; i.e., no lines are considered. Model 2 is a classical H-He NLTE/L model where all hydrogen and He II lines are considered. Model 3 considers in addition the C IV lines, and model 4 includes all lines of H I, He II, C IV, Fe IV, Fe V, and Fe VI. The run of temperature for all models versus column mass is displayed in Figure 14. The effect of lines is similar to the previously discussed case of an early B star. Again, the surface cooling due to the iron lines is appreciable; however, most of the cooling at $-4 < \log m < -2$ with respect to the H-He model is provided by the C IV lines rather than by the iron lines. A similar conclusion was also reached by Dreizler & Werner (1993), who have presented illustrative results for a similar effective temperature (although at higher log g). Finally, we present in Figure 15 the non-LTE and LTE ionization balance of iron. We see that the non-LTE effects on the iron ionization are important as pointed out by Dreizler & Werner (1993). This finding has profound implications for the interpretation of spectra. We shall return to this point in subsequent papers of this series, where we will study in detail models and spectra of hot white dwarfs and hot O subdwarfs.

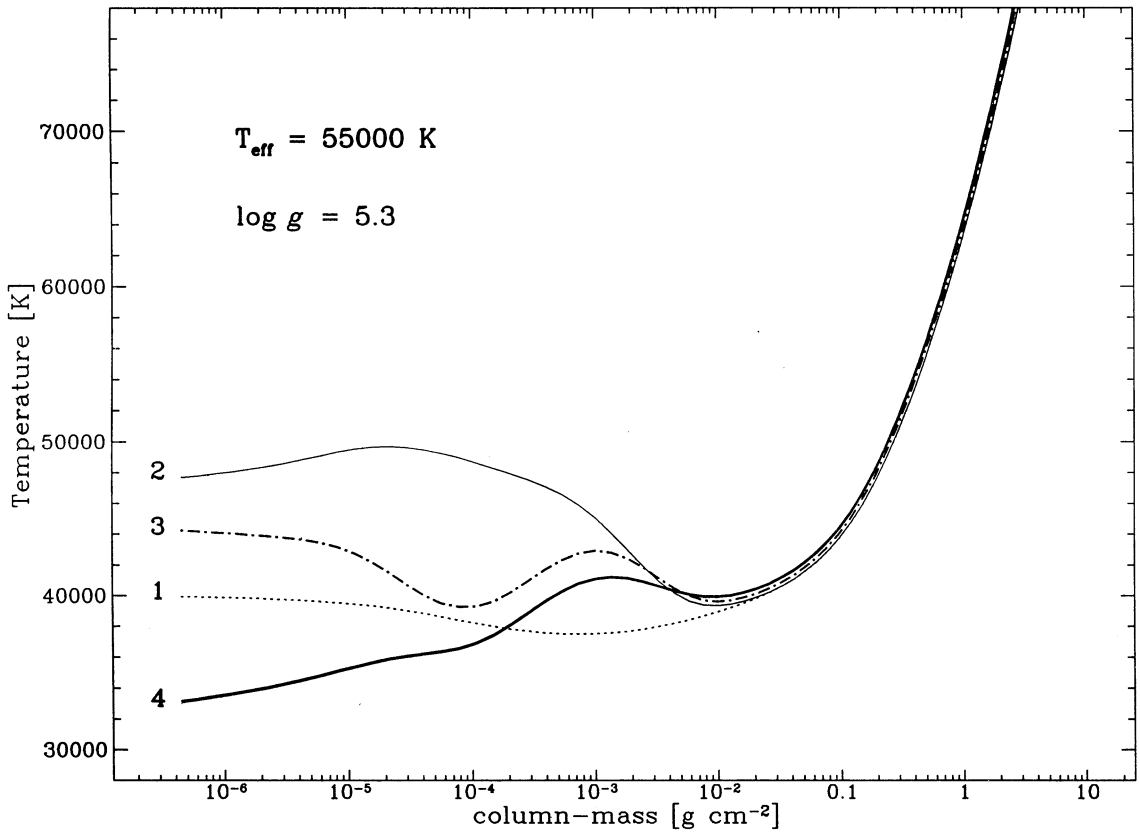

FIG. 14.—Plot of the temperature vs. column mass for various model atmospheres T_{eff} = 55,000 K; log g = 5.3 (a typical hot O subdwarf: see Table 11). Model 1, simple H-He NLTE/C model (no lines considered); model 2, He-He NLTE/L model (all lines of H and He considered), model 3, H-He-CNO model, only H, He, and C IV lines considered; model 4, H-He-CNO-Fe model, all lines (H, He, C IV, and Fe IV to Fe VI) are considered

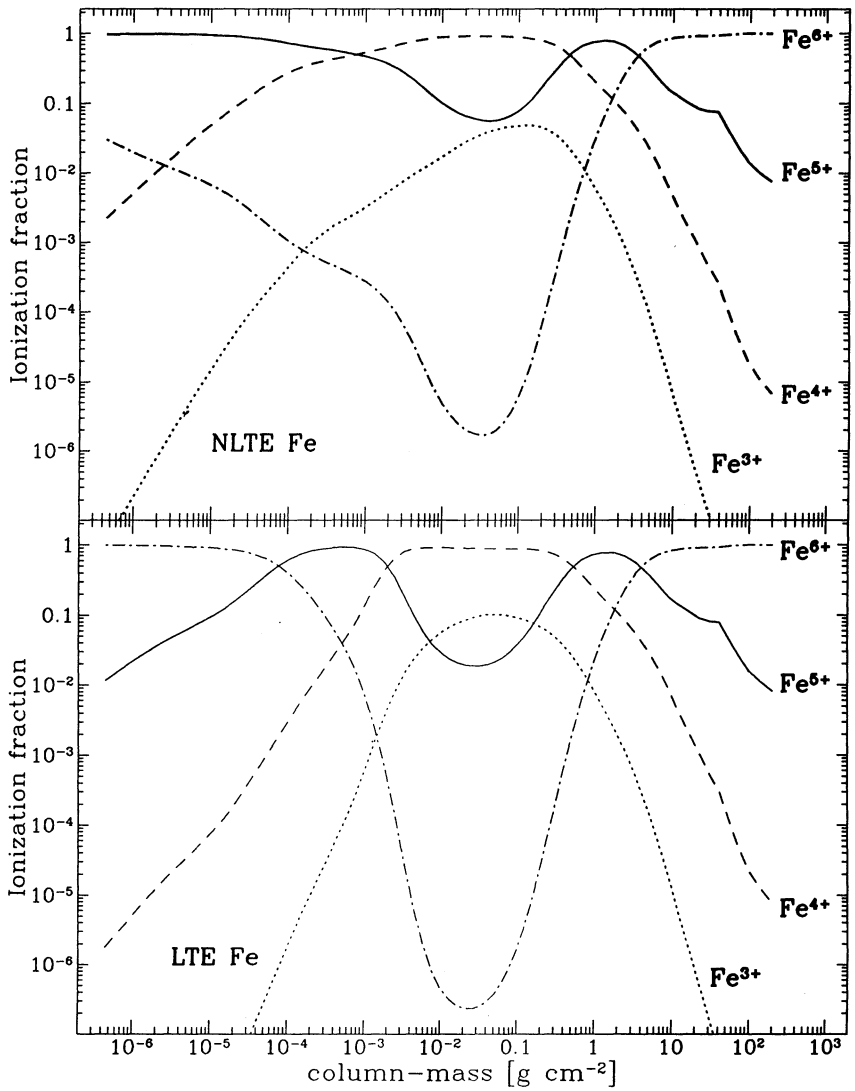

FIG. 15.—Non-LTE (*upper panel*) and LTE (*lower panel*) ionization balance of iron. The individual ionization fractions for four ions of iron, Fe^{3+} to Fe^{6+}, are plotted as functions of the column mass. The non-LTE total number densities for the individual iron ions were calculated by summing all corresponding non-LTE level populations together with LTE "upper sums" for model 4; the LTE ionization balance was calculated by the Saha equation for the structure of the H-He NLTE/L model (model 2), which is what would the "classical" non-LTE unblanketed model predict.

5. DISCUSSION

The hybrid CL/ALI method may be viewed as an improvement over both the complete linearization method, and the ALI scheme.

Improvement over the original CL method is obvious. As was demonstrated in § 4.1, even a relatively simple NLTE/L model requires much more computer time for completing one iteration of the standard CL than for the fully converged model calculated with the hybrid scheme. However, this comparison is not entirely fair. It was long ago recognized that not all the frequency points have to be linearized within the context of the CL method. This idea was applied consistently in the original versions of TLUSTY (Hubeny 1988) where the notion of "fixed frequencies" was fully utilized. We stress that, in the present terminology, the implementation of this idea is nothing else than a variant of the present hybrid scheme with all the "ALI" frequency points considered as "fixed" frequencies, with $\Lambda^* = 0$. In other words, the fixed-frequency approach simply means that the radiation field in these frequencies is treated by means of the classical lambda iteration. An obvious drawback to this approach is that it converges much more slowly than the ALI scheme. To demonstrate this, we calculate a model analogous to NLTE/L model C (§ 4.1)—Figure 16. We see that the convergence is indeed substantially faster when using the ALI treatment of previously "fixed" frequency points.

We now turn to discussion of the second point, namely how the hybrid scheme improves the original ALI method. Again, the answer is obvious—the hybrid scheme increases the convergence rate considerably, while it keeps the time per iteration essentially unchanged with respect to the standard ALI.

The problems of slow convergence of ALI have been discussed by several authors. For instance, Pauldrach & Herrero (1988, their Fig. 5) have suggested an improvement of the convergence properties by using a special preconditioning procedure, which uses

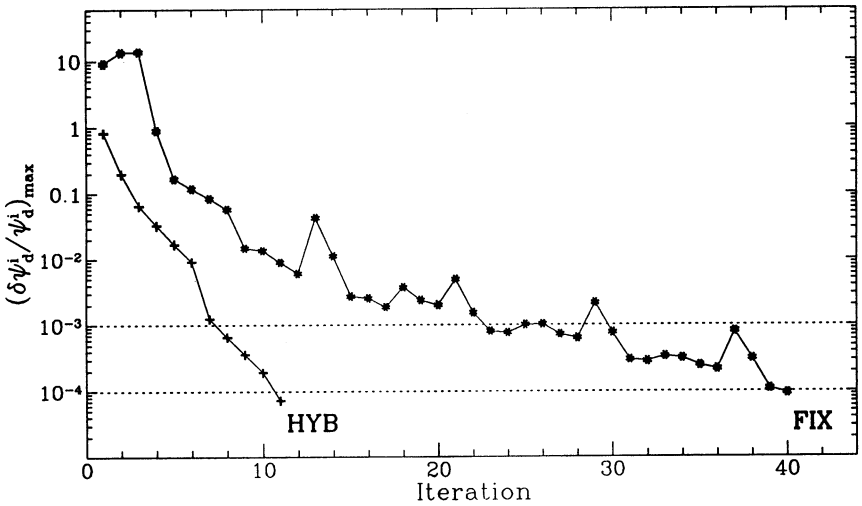

FIG. 16.—A comparison of the "fixed frequency" approach and the hybrid CL/ALI approach for models analogous to those displayed in Fig. 9 (NLTE/L models for the standard test case atmosphere). Model labeled "FIX" was calculated assuming radiative rates in all lines but Lyα, Lyβ, Lyγ, and Hα to be fixed, while the model labeled "HYB" treated the corresponding frequency points by means of the ALI approach. See the text for details

information not only from the previous iteration step, but also from one still earlier iteration. Another possibility for improving the convergence rate is to apply a tridiagonal Λ^* operator instead of a diagonal one (Werner 1988; Hillier 1990). This idea was suggested originally by Olson & Kunasz (1987), who have demonstrated numerically that the use of tridiagonal operator speeds up the convergence considerably. The explanation is easy—by using a tridiagonal operator, one allows for a depth coupling of the radiation intensities explicitly, while when using a diagonal (local) operator, depth coupling is treated only via the correction term ΔJ^{old} (see equation [8]). This kind of behavior is present even in the simple so-called restricted non-LTE problem—a simultaneous solution of the radiative transfer and statistical equilibrium equations, assuming the temperature and density are fixed. In the case of stellar atmosphere models, the problem is more serious because the set of equations to be solved simultaneously includes also the radiative and hydrostatic equilibrium equations. Hillier (1990) has presented an illuminating discussion of this problem. He has shown that when invoking the diffusion approximation, which correctly describes the behavior of the radiation intensity at large depths, we obtain

$$(J - S) \approx \frac{1}{3}\frac{d^2S}{d\tau^2}, \tag{53}$$

which is explicitly nonlocal, and therefore is better approximated by a tridiagonal than a diagonal operator. The left-hand side of equation (53) is in fact an integrand of the radiative equilibrium (RE) equation when written in the integral form (see equation [11] and subsequent discussion). Therefore, when only the integral form of RE is used, the tridiagonal operator enhances the convergence rate considerably.

However, the present hybrid CL/ALI scheme offers a different method of coping with the problem of depth coupling. Since the radiation intensities at the most important frequencies are treated by linearizing the *exact* transfer equation, the depth coupling in these points is already treated fully self-consistently. Moreover, concerning the radiative equilibrium, we use here a combination of the integral and the differential forms (eq. [11]), which is moreover dominated by the latter at large depths. Since the differential form takes the depth coupling into account explicitly, even for the diagonal operator, the use of a tridiagonal operator is not so crucial in the context of our scheme. Therefore, we do not expect that a tridiagonal operator will bring an essential improvement. However, we are currently working on implementing a tridiagonal operator to our scheme, and the preliminary tests indeed verify this hypothesis: while for the pure ALI scheme the tridiagonal operator yields a significantly better convergence, it does not result in any significant improvement in the hybrid case. In fact, although the tridiagonal operator produces a converged solution in a slightly smaller number of iterations, the time per iteration is appreciably larger (because of the extra time needed for setting up and multiplying necessary matrices), so that the total time is larger. Nevertheless, we are still working on optimizing and debugging the code; the final results may change these preliminary conclusions. The results will be presented in a future paper.

Besides the problem of depth coupling, there is another, and perhaps more important, problem connected with the application of ALI to constructing model stellar atmospheres. When using complete linearization, both the radiation intensities, as well as the optical depth scale, are explicitly linearized, and therefore allowed to change in a given linearization iteration. On the other hand, the approximate Λ^* operator, whether diagonal or tridiagonal, is evaluated on an optical depth scale corresponding to the current iteration (i.e., with the "old" populations) and is *not allowed* to change during the given linearization iteration. In other words, the ALI scheme improves the situation over the classical lambda iteration (or, in the present context, over the idea of "fixed" frequencies) by allowing the radiation field to vary during the linearization iteration (via expressing S through eq. [8] and linearizing the source function), but it does not similarly allow one to vary the optical depth scale, which is in fact treated by means of the classical lambda iteration (i.e., updated only *after* a completed linearization iteration step).

A possible solution of this problem is to explicitly linearize Λ^* with respect to the monochromatic optical depth, which in turn is easily linearizable with respect to the temperature, electron density, and populations. Another possibility is to employ the idea of an

TABLE 12

DESCRIPTION OF THE MODELS CALCULATED WITH THE EQUIVALENT TWO-LEVEL ATOM APPROACH AND ACCELERATION PROCEDURES WITHIN THE ALI SCHEME[a]

		NG ACCELERATION	
Model	ETA	Start	Step
B1.....	None	97	4
B2.....	Hα, Lyγ, Lyβ, Lyα	97	4
B3.....	None	7	4
B2.....	Hα, Lyγ, Lyβ, Lyα	7	4

[a] Models are analogous to NLTE/L models of Table 9.

approximate Newton-Raphson operator (Schönberg & Hempe 1986; Hillier 1990), which takes linearization of the optical depth scale into account automatically. We are currently working on incorporating an explicit linearization of Λ^* to our code.

A partial, but not very efficient, solution of this problem is to apply the idea of the equivalent-two-level atom (ETA) approach (see, e.g., Mihalas 1978). It was shown by Hubeny (1988) that this approach significantly improves the convergence of the standard CL method, because it provides a more consistent solution of the radiative transfer and statistical equilibrium equations between the individual linearization iterations. As follows from the above discussion, such a procedure, applied for the most important transitions, should also improve the convergence of the ALI scheme, because it replaces the lambda-iteration type treatment of the monochromatic optical depth by the ETA treatment.

To study the effects of ETA applied between the individual iterations, in connection with various acceleration schemes, we have calculated several models by applying the full ALI, analogous to the NLTE/L model B from § 4.1.3 (i.e., non-LTE H-He model with lines)—see Table 12 and Figures 17*a* and 17*b*. In all the following models, the Kantorovich acceleration is switched on after the fourth iteration. Model B1 represents the "pure" ALI scheme—no ETA procedure between iterations, and no Ng acceleration till the 97th iteration, when we perform one to demonstrate its effect on an almost converged model. We see that it indeed has a significant effect. Model B2 is analogous to B1 as far as the Ng acceleration is concerned but differs from it by performing the ETA procedure for Hα, Lyγ, Lyβ, and Lyα (in this order), and repeating this series twice (i.e., altogether eight ETA procedures) after each completed linearization iteration. Model B3 applies the Ng acceleration in our standard manner—started after the seventh iteration and performed every four iterations; while it does not apply any ETA procedure. Model B4 employs the same Ng acceleration strategy as B3, but applies the ETA procedure as in B2. We see that both, the Ng acceleration and the ETA procedure, individually or together, improve the convergence of the pure ALI scheme. In particular, applying both of them simultaneously (model B4) yields a relatively rapid convergence. It is noteworthy that unlike the experience of other workers (e.g., Werner 1988; Kubat 1994), who have found the Ng acceleration not to be very helpful in the ALI model atmosphere codes, even leading is some cases to divergence, in our experience the Ng acceleration either indeed accelerates, or at worst does not help very much, but never decelerates the convergence.

The above notwithstanding, we do not consider the ETA approach to be the most efficient way to improve the convergence properties of the full ALI scheme because, unlike the Ng acceleration, it is relatively time-consuming. To demonstrate this, we plot in Figure 17*b* the timing for all models. Performing eight ETA procedures increases the time per iteration almost twice (for a pure ALI method, the computer time is dominated by the formal solution). But these results indicate that any method which is capable of providing a fast, self-consistent solution of the radiative transfer plus statistical equilibrium, keeping the temperature and electron density fixed, may be used here. An example of such a method is another application of ALI, with a preconditioning of the statistical equilibrium (Rybicki & Hummer 1991).

We stress, once again, that these strategies of dealing with convergence problems are most needed for the full ALI scheme. Our newly developed hybrid CL/ALI method, accompanied by "low-cost" accelerations (Ng and, above all, Kantorovich) provides a more attractive method than any variant of the full ALI treatment (compare Fig. 17*b* to Fig. 9*b*).

6. CONCLUSIONS

We have developed a new numerical method for computing sophisticated non-LTE model stellar atmospheres. The method combines the advantages of its two basic constituents: its rate of convergence is practically as high as for the standard complete linearization method, while the computer time per iteration is essentially as low as in the standard ALI method. We therefore call this the hybrid CL/ALI method.

The method formally resembles the standard complete linearization; the only difference is that the radiation intensity at some (or possibly all) frequency points is not linearized; instead, it is treated by means of the ALI approach. The choice of frequency point partitioning is completely specified by the user and may range from the pure complete linearization to pure ALI method.

Compared to the standard, even accelerated, complete linearization, the gain in computer time is enormous, but more interestingly, the hybrid method, with only a very small number of frequency points to be linearized, is both faster and more accurate than the full ALI scheme. Essentially, the reason is that while the full ALI scheme treats the depth coupling of radiation intensities *iteratively* (via the "correction" term of eq. [7]), the hybrid scheme considers the depth coupling in a few of the most important frequency points *explicitly*. The very basis of the method is thus to select the "explicit" points in the most efficient way. We have demonstrated that a simple, but reasonable, strategy is to consider a few (two to four) frequencies in the most opaque parts of the

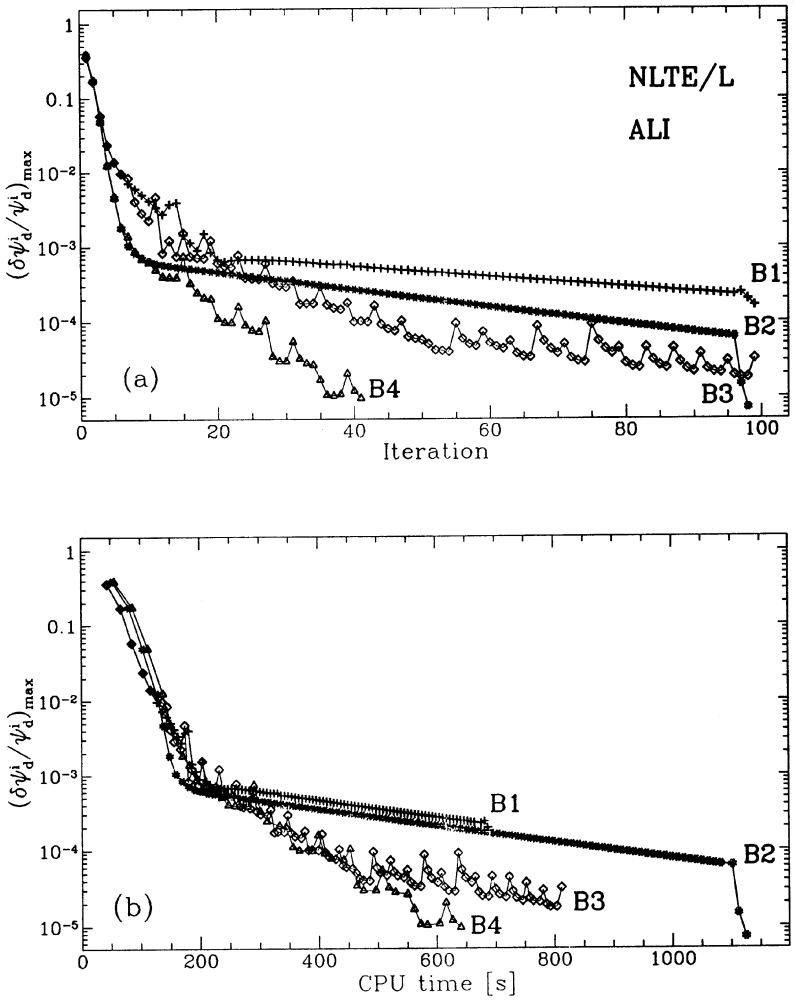

FIG. 17.—Effect of the Ng acceleration and the equivalent-two-level-atom (ETA) procedures on the convergence properties of NLTE/L models calculated by the full ALI scheme (see Table 12). Models are analogous to those displayed in Fig. 8 (*a*) The maximum relative change is plotted as a function of the iteration number; (*b*) the maximum relative change is plotted as a function of the total CPU time at the end of every iteration step. Model B1, no Ng acceleration till the 97th iteration; no ETA procedures. Model B2, no Ng acceleration till the 97th iteration; ETA procedures (see the text). Model B3, Ng acceleration (7/4); no ETA. Model B4, Ng acceleration (7/4); ETA procedures. In all models, the Kantorovich acceleration is started at 4th iteration. Notice a significant effect of the Ng acceleration at the 97th iteration for models B1 and B2

most important transitions as explicit. For instance, for the test calculations reported in § 4.1 we found that considering four frequency points in the Lyman continuum, and two points per the first three Lyman lines and the first Balmer line, provides a nearly optimum set of "explicit" frequencies.

Finally, we have shown that this method can be applied to calculating fully line-blanketed non-LTE model atmospheres, by using the idea of "superlevels" and "superlines" introduced originally by Anderson (1989). We have extended and generalized Anderson's approach by treating consistently the level dissolution by means of the non-LTE occupation probability treatment developed earlier (Hubeny et al. 1994). We have further developed the concept of opacity distribution functions and have discussed at length the various strategies to deal with the serious problem of the overlap of different distribution functions. Finally, we have calculated several illustrative model atmospheres taking into account several tens of thousand of lines of Fe III to Fe VI in non-LTE. These results demonstrated that the present hybrid CL/ALI method indeed provides a robust method for calculating non-LTE line-blanketed model atmospheres for a wide range of stellar parameters. The results for individual stellar types will be presented in forthcoming papers in this series.

We thank Bruce Altner for careful reading of the manuscript and for many useful suggestions. This work was supported in part by NASA grants NAGW-3025 and NAGW-3834.

REFERENCES

Anderson, L. S. 1985, ApJ, 298, 848
———. 1987, in Numerical Radiative Transfer, ed. W. Kalkofen (Cambridge: Cambridge Univ. Press), 67
———. 1989, ApJ, 339, 588
———. 1991, in Stellar Atmospheres: Beyond Classical Models, ed. L. Crivellari, I. Hubeny, & D. G. Hummer (NATO ASI Series C 152)(Dordrecht: Kluwer), 29
Auer, L. H. 1991, in Stellar Atmospheres: Beyond Classical Models, ed. L. Crivellari, I. Hubeny, & D. G. Hummer (NATO ASI Series C 152) (Dordrecht: Kluwer), 9
Auer, L. H., Heasley, J. N., & Milkey, R.W. 1972, Kitt Peak Obs. Contr., No. 555
Auer, L. H., & Mihalas, D. 1969, ApJ, 158, 641
———. 1970, MNRAS, 149, 65
Cannon, C. J. 1973a, J. Quant. Spectrosc. Rad. Transfer., 13, 627
———. 1973b, ApJ, 185, 621
Carbon, D. F. 1984, in Methods in Radiative Transfer, ed. W. Kalkofen (Cambridge: Cambridge Univ. Press), 395
Carlsson, M. 1986, Report No. 33 (Uppsala: Uppsala Astron. Obs.)
Cassinelli, J. P., et al. 1995, ApJ, 438, 932
Crivellari, L., Hubeny, I., & Hummer, D. G. 1991, Stellar Atmospheres: Beyond Classical Models (NATO ASI Series C 152) (Dordrecht: Kluwer)
Dreizler, S., & Werner, K. 1992, in Lecture Notes in Physics, 401, The Atmospheres of Early Type Stars, ed. U. Heber & C. S. Jeffery (Berlin: Springer-Verlag), 436
———. 1993, A&A, 278, 199
Heap, S. R., Hubeny, I., Lanz, T., & Altner, B. 1992, BAAS, 24, 1203
Herrero, A. 1987, A&A, 171, 189
Hillier, D. J. 1990, A&A, 231, 116
Hubeny, I. 1986, in IAU Colloq. 90, Upper Main Sequence Stars with Anomalous Abundances, ed. C. R. Cowley, M. M. Dworetsky, & C. Mégessier (Dordrecht: Reidel), 57
———. 1988, Comput. Phys. Comm., 52, 103
———. 1992, in Lecture Notes in Physics, 401, The Atmospheres of Early Type Stars, ed. U. Heber & C. S. Jeffery (Berlin: Springer-Verlag), 377
Hubeny, I., Hummer, D. G., & Lanz, T. 1994, A&A, 282, 157
Hubeny, I., & Lanz, T. 1992, A&A, 262, 501
———. 1993a, in IAU Colloq. 138, Peculiar versus Normal Phenomena in A-Type and Related Stars, ed. M. M. Dworetsky, F. Castelli, & R. Faraggiana (ASP Conf. Ser., 44), 98
Hubeny, I., & Lanz, T. 1993b, BAAS, 25, 878
Kubat, J. 1994, A&A, 287, 179
Kudritzki, R. P., & Hummer, D. G. 1990, ARA&A, 28, 303
Kurucz, R.L. 1979, ApJS, 40, 1
———. 1991, in Stellar Atmospheres: Beyond Classical Models, ed. L. Crivellari, I. Hubeny, & D. G. Hummer (NATO ASI Series C 152) (Dordrecht: Kluwer), 441
———. 1992, in IAU Symp. 149, The Stellar Populations of Galaxies, ed. B. Barbuy & A. Renzini (Dordrecht: Kluwer), 225
Lanz, T., & Hubeny, I. 1995, ApJ, 439, 905 (Paper II)
Lanz, T., Hubeny, I., Cheng, F.-H., & Horne, K. 1992, BAAS, 24, 1203
Mihalas, D. 1978, Stellar Atmospheres (San Francisco: Freeman)
Mihalas, D., Heasley, J. N., & Auer, L. H. 1975, A Non-LTE Model Stellar Atmospheres Computer Program, NCAR-TN/STR-104 (MHA)
Olson, G. L., Auer, L. H., & Buchler, R. 1986, J. Quant. Spectrosc. Rad. Transf., 35, 431
Olson, G. L., & Kunasz, P. B. 1987, J. Quant. Spectrosc. Rad. Transf., 38, 325
Pauldrach, A., & Herrero, A. 1988, A&A, 199, 262
Peytremann, E. 1974, A&A, 33, 203
Rybicki, G. 1972, in Line Formation in the Presence of Magnetic Fields, ed. R. G. Athay, L. L. House, & G. Newkirk (Boulder: High Altitude Obs.), 145
———. 1991, in Stellar Atmospheres: Beyond Classical Models, ed. L. Crivellari, I. Hubeny, & D. G. Hummer (NATO ASI Series C 152) (Dordrecht: Kluwer), 1
Rybicki, G., & Hummer, D. G. 1991, A&A, 245, 171
———. 1992, A&A, 262, 209
Scharmer, G. 1982, ApJ, 249, 720
Schönberg, K., & Hempe, K. 1986, A&A, 163, 151
Sneden, C., Johnson, H. R., & Krupp, B. M. 1976, ApJ, 204, 281
Sparks, W. M., & Fischel, D. 1971, Partition Functions and Equations of State in Plasmas (NASA-SP 3066) (Washington: NASA)
Werner, K. 1986, A&A, 161, 177
———. 1987, in Numerical Radiative Transfer, ed. W. Kalkofen (Cambridge: Cambridge Univ. Press), 67
———. 1988, A&A, 204, 159
———. 1989, A&A, 226, 265
Werner, K., & Husfeld, D. 1985, A&A, 148, 417